Realistic μPMU Data Generation for Different Real-Time Events in an Unbalanced Distribution Network

Medattil Ibrahim, Abdul H.; Sharma, Madhu; Subramaniam Rajkumar, Vetrivel

DOI
10.3390/en16093842

Publication date
2023

Document Version
Final published version

Published in
Energies

energies

MDPI

Article

Realistic μPMU Data Generation for Different Real-Time Events in an Unbalanced Distribution Network

Abdul Haleem Medattil Ibrahim [1,2,*], Madhu Sharma [1] and Vetrivel Subramaniam Rajkumar [2]

[1] Department of Electrical and Electronics Engineering, University of Petroleum and Energy Studies, Dehradun 248007, India; madhusharma@ddn.upes.ac.in
[2] Department of Electrical Sustainable Energy, Delft University of Technology, 2628 CD Delft, The Netherlands; v.subramaniamrajkumar@tudelft.nl
* Correspondence: abdulhaleem.powerresearcher@ieee.org

Abstract: Monitoring, protection, and control processes are becoming more complex as distributed energy resources (DERs) penetrate distribution networks (DNs). This is due to the inherent nature of power DNs and the bi-directional flow of current from various sources to the loads. To improve the system's situational awareness, the grid dynamics of the entire DER integration processes must be carefully monitored using synchronized high-resolution real-time measurement data from physical devices installed in the DN. μPMUs have been introduced into the DN to help with this. In comparison to traditional measurement devices, μPMUs can measure voltage, current, and their phasors, in addition to frequency and rate of frequency change (ROCOF). In this study, an approach to generating realistic event data for a real utility DN utilizing strategically installed μPMUs is proposed. The method employs an IEEE 34 test feeder with 12 μPMUs installed in strategic locations to generate real-time events-based realistic μPMU data for various situational awareness applications in an unbalanced DN. The node voltages and line currents were used to analyze the various no-fault and fault events. The author generated the data as part of his PhD research project, utilizing his real-time utility grid operation experience to be used for various situational awareness and fault location studies in a real unbalanced DN. The DN was modeled in DIgSILENT PowerFactory (DP) software. The generated realistic μPMU data can be utilized for developing data-driven algorithms for different event-detection, classification and section-identification research works.

Keywords: μPMUs; real-time events; data generation; distribution network; fault events; situational awareness; modeling and simulation; load flow analysis; RMS simulation

Citation: Medattil Ibrahim, A.H.; Sharma, M.; Subramaniam Rajkumar, V. Realistic μPMU Data Generation for Different Real-Time Events in an Unbalanced Distribution Network. *Energies* **2023**, *16*, 3842. https://doi.org/10.3390/en16093842

Academic Editors: Theofilos A. Papadopoulos and Eleftherios O. Kontis

Received: 22 March 2023
Revised: 25 April 2023
Accepted: 26 April 2023
Published: 29 April 2023

1. Introduction

In the past, when radial power distribution and one-way power flow were prevalent, it was sufficient to evaluate the design conditions' envelope, such as peak loads or fault currents, rather than continuously monitoring the operational status. However, as DERs are integrated on a large scale, fluctuation, unpredictability, and the potential to enlist a variety of resources for grid services present themselves, sparking demand for tools such as sophisticated sensors and much more extensive monitoring in order to accurately observe, comprehend, and manage the DN [1]. The SCADA (supervisory control and data acquisition) system is used by the majority of electric utilities around the world to monitor and control electric power DN. RTUs, which are traditional measurement devices installed throughout the power system, transmit data to the SCADA system. With a low resolution, it records unsynchronized voltage, current magnitude, and real and reactive power flow (a few seconds). As a result, the SCADA system is unable to capture the dynamic behavior of the current DN [2]. Because of the large number of nodes, short distances, small amplitude and angle differences between nodes, unbalanced loads, and faster dynamics, DN is extremely complex. Because of the inherent complexities, there is a greater need for the development of new high-accuracy and precision monitoring systems that support

situational awareness in the DN. This enables distribution operators to respond to such disturbances by making operational decisions [3]. To improve situational awareness and alleviate these complexities, the micro-phasor measurement unit (μPMU) was developed for DN [4]. μPMU generates time-synchronized voltage and current phasors in real time with high accuracy, precision, and sampling rate. Synchronization is accomplished by simultaneously sampling voltage and current phasors with GPS receiver timing signals [5]. It has a precision angle of 0.01, a total vector error allowance of 0.05%, an angle resolution of 0.002, and a magnitude resolution of 0.0002% [6]. Its sampling rate can be adjusted from 10 to 120 samples per second for a 60 Hz system [7]. Operators can monitor distribution applications in real time due to the high performance of μPMU technology in DN.

With the expansion of sensor data comes new challenges, such as how to handle data anomalies, enable real-time processing, and control cyber security [8]. The limited control center uses of μPMU measurements show that, overall, translating high-resolution μPMU data into real-time actionable information remains an important challenge [9]. A single-line-to-neutral fault at a real DN in Riverside, CA, is investigated using data from five μPMUs to conduct a detailed analysis of how faults affect different voltage levels [10]. Due to the infrequent, unscheduled, and unknown nature of the events, a large volume of PMU data contains a large number of events that are difficult to analyze [11]. Some techniques improve awareness by combining data from various monitoring devices installed in the network. Using data from smart meters and μPMUs, [12] examines real-time topology detection and state estimation in DN. An impedance-based method is demonstrated in [13] that computes fault currents using observed voltages measured by μPMUs and known bus impedance before employing distributed parameters to calculate the fault distance from the measured site. The addition of μPMU devices in specific distribution system sites was investigated in [14] to enrich smart meter data with high-resolution data and improve time-series estimations. The work in [15] performs a thorough investigation of how various voltage levels are affected by capacitor-bank-switching events in DN using data-driven experimental analysis on a capacitor-bank-switching event in a real DN using μPMU data. In circuit theory, the compensation theorem serves as the foundation for a technique that generates an equivalent circuit to describe the event using voltage and current synchrophasors recorded by μPMUs [16]. The fault source location is determined by performing an improved distribution system state estimation in a hierarchical structure based on the feeder graph model in the decreased searching zone [17]. In [18], for the event categorization approach, the wavelet transforms and shifts in the magnitudes and phase angles of the voltage and current phasors are used. A method for determining whether a frequency event is propagated from the transmission system formed within a DN or erroneously generated by instantaneous frequency estimation algorithms is tested utilizing real μPMU data [19]. Most of the investigations are carried out using μPMU data. When combining high-quality and high-resolution μPMU data with conventional measurements, it is difficult to obtain the best state-estimation scheme, and the software will require more processing power. The system's computational load rises as additional devices that require measurement are added, which increases the data volume [20].

The use of these data has been described in numerous works; however, all the relevant real-time events have not fully been investigated with specified abnormalities and events. Field data are challenging to collect and are not marked for abnormalities or incidents [9]. Besides the real data-handling challenges of μPMUs, due to privacy and security concerns, accessing field data is exceedingly difficult. These challenges are the roadblocks for researchers who explore the benefits of the μPMU data in the context of highly dynamic, unbalanced DN. This study describes a technique for producing accurate μPMU data for the specified IEEE benchmark network. We must put our tools to the test on accurate μPMU data to determine how well they will operate in the actual world [9].

There are a few open-source data sets that have been documented in the literature; however, they either have a short access duration, a difficult process, or are only available to collaborators. As a result, there is still a problem and a gap in the research, but the authors

were driven to produce accurate data from a benchmark dataset that was readily available. The author utilizes his real-time distribution grid operation experience to generate these data and carry out applied research in the field of DN situational awareness improvement techniques for distribution control center (DCC) operators. The goal of this work is to generate realistic real-time events-based μPMU data that can be utilized to develop different real-time monitoring applications for the DN. The applications developed using these data can be utilized to enhance the visibility of the network. The main contributions of this paper are as follows:

1. Modeling an unbalanced real distribution network in DP. This model is subsequently used for data generation.
2. Synthetic μPMU data generation for real-time applications, such as event detection, classification and localization.
3. Validation of the generated data with real data published in the literature and with the load flow variations in the network.

The paper is organized with real-time events described in Section 2, followed by the real-time event-based data-generation methodology in Section 3. The results of the generated events are discussed in Section 4. Section 5 presents the validation of the generated data. An experimental use case is tested in Section 6 utilizing the generated realistic data. Section 7 summarizes the conclusions.

2. Real-Time Events in DN

All the DN are designed as meshed networks but with radial operating structures and unbalanced load connections, hence the name unbalanced network. The complexity of the issue is further increased by the non-linear power flow, the scale of the networks, and switching choices [21]. The real DN is prone to various events. Fault events and no-fault events are the main categories of real-time events. The events in a DN network can be defined as the act of connecting or disconnecting the components from the network due to the normal and abnormal conditions of the components or the networks themselves. A detailed list of the no-fault and fault events that normally happen in the real utility DN is listed below.

2.1. No-Fault Events

These categories of events are the normal events or planned events happening in the real DN as a part of its network operation or maintenance requirements. Load switching is one of the most common events in the real DN. Any abnormality in the load-connected circuit or the connected equipment that causes the load to trip or get disconnected is called load switching. The impact of this will be reflected in the total load currents per phase and even in the line currents and node voltage. These variations in the line currents are due to the switching of unbalanced loads. Another important and common event that happens in the real network is the capacitor bank switching. Utilities use reactive power compensation techniques to use equipment that generates local reactive power at the distribution level to make up for the necessary reactive power and obtain near-ideal power factor values [15]. With the increased penetration of different energy resources to the grid, DER integration has become a common trend for distribution because of the low-voltage (LV) integration flexibility. Although the DER installations support the DN during the required times, the inverter-based DERs pose a wide range of challenges to the grid operators and even the customers in terms of the quality and continuity of the services. Hence, DER or DG (distributed generation) switching is to be considered as yet another important dynamic event of the DN that is to be monitored and controlled very closely. Planned and unplanned transformer outages are another real-time event in the distribution grid. This transformer includes primary substation transformers, line transformers and load-level or customer-level distribution transformers (DTs). During planned outages, the transformer is de-energized from the LV side and then from the high-voltage (HV) side, based on the availability of CBs or fuse switches. After the proper isolation

and grounding of the transformer, either the equipment is checked and repaired as a part of routine or preventive maintenance, or is repaired for a major defect that is determined during the condition monitoring of the equipment and parts. This is considered a periodic event in the DN in case of routine or scheduled transformer maintenance but an unplanned or emergency outage in the case of a major defect on the transformer. When transformers are kept out of service, the loads connected to them are also out of service automatically, and the impact is reflected in the node voltages as well as the line currents. So, these variations need to be distinguished and identified using a reliable and high-resolution monitoring device to capture and identify the transformer disconnection dynamics. Voltage-regulation events, popularly known as tap-changer events, are yet another common event that occurs in the DTs of the DN, where the busbar voltages of the different levels are kept within the limits either by lowering or raising the taps using on-load and off-load tap changers. Even though the tap-changer events have less impact on the line currents, the voltage variations can be observed at the corresponding nodes. All these events described above are considered normal events, as they do not trigger the protection devices that work on crossing the set points.

2.2. Fault Events

Unlike normal events, a fault event is an abnormal condition, caused by any power system component failures, human errors and environmental conditions, thus leading to an abnormal current flow through the network. Among the four parts of the power system, DN has the most interruptions, accounting for 80% of all interruptions. Real-time DN fault events can be split into two categories: transient and permanent, with transient faults making up 80% and permanent faults 20% of total fault events [22]. Transient faults mostly happened during extreme weather conditions and also mainly on the overhead lines (OHLs) and associated equipment. The normal procedure adopted by the utilities when a transient fault happens on the DN is reclosing the line either through the auto-recloser installed at the feeder's heads or by closing the feeder CBs from the SCADA systems. If the breaker is closed after reclosing, then the fault is confirmed as a temporary or transient fault. However, if the breaker is tripped again, then the fault is confirmed to be a permanent fault. Most of the transient faults restorations lead to an open circuit fault in the OHL, as the reclosing surges weaken and open the OHL jumper connections between the overhead line poles. The four primary types of short circuit faults—line to ground (LG), line to line (LL), double line to ground (DLG), and three line to ground (LLLG)—are regarded as permanent faults [23].

3. Methodology

The realistic data-generation methodology basically considers the possibilities of creating all the realistic events planned as per the author's real-time DN operation experience and data availability to model the network in the modeling and analysis tool. The main challenge faced during the formulation of the methodology is the implementation of real-time events to keep the data more realistic in nature. However, the challenge was addressed by selecting the best-suited network from the available reliable sources and a capable network modeling and analysis tool. The methodology employed in this study consisted of a rigorous seven-step process to analyze the behavior of a real-world DN. The first step involved selecting and modeling the real DN. Next, load flow analysis was performed on the network, with the results being validated against published results to ensure accuracy. Following this, μPMUs and DGs were strategically placed within the network to enable the precise monitoring of system behavior. Real-time events were then defined and their settings configured, with careful attention paid to ensuring that the event types and parameters are representatives of real-world scenarios. The data-generation settings were also established to generate accurate and representative data. Subsequently, the simulation of the different real-time events was performed, and the results were plotted for analysis. Finally, the data were validated to ensure that the results are reliable and accurate.

3.1. Real DN Selection and Modeling

Out of the available benchmark test feeders, the IEEE 34 node test feeder qualified as the best candidate for the analysis. This feeder is a real DN that is situated in Arizona. The system voltage of the feeder is 24.9 kV. The feeder is distinguished by its length and light load, the need for two in-line regulators to retain the specified voltage limits, and other factors. The DN has the inherent nature of unbalanced loading with both "spot" and "distributed" loads and shunt capacitors, an in-line transformer decreasing the voltage for a shorter portion of the feeder to 4.16 kV [24]. The feeder's length and the unbalanced loading could help to generate realistic dynamics on the DN and visualize using the high-resolution data-measurement capability of µPMUs.

The test feeder is modeled using DP to create real-time events and scenarios. The IEEE 34 node is perfectly modeled using the feeder components data given in [25]. The DP has a rich components library and features that helped to model the network without any assumptions in connecting the components. The DP supports the modeling of three-phase, four-wire systems, which are very important in modeling the unbalanced three-phase DN [26,27]. The spot loads are placed at the nodes, and the distributed loads are connected at the middle of the line. The line sections of the network are labeled as shown in Table A1 of Appendix A.

The feeder is modeled without a substation transformer, as the load flow results published do not consider it for generating load flow results. However, an external grid connection with 1.05 p.u as reference phase-to-phase voltage for the base node 800 is selected for this study. The voltage regulator (VR) tap positions are kept as 12-05-05 (A-B-C) and 13-11-12 (A-B-C) for regulators 1 and 2, respectively. Figure 1 shows the test feeder modeled in DP. The phase A-N connection is represented by the components with red dotted lines, phase B-N connections are shown by yellow dotted lines, phase C-N connections are shown by blue dotted lines, and phase ABC-N connections are shown by black dotted lines. The components highlighted in grey color are the DGs.

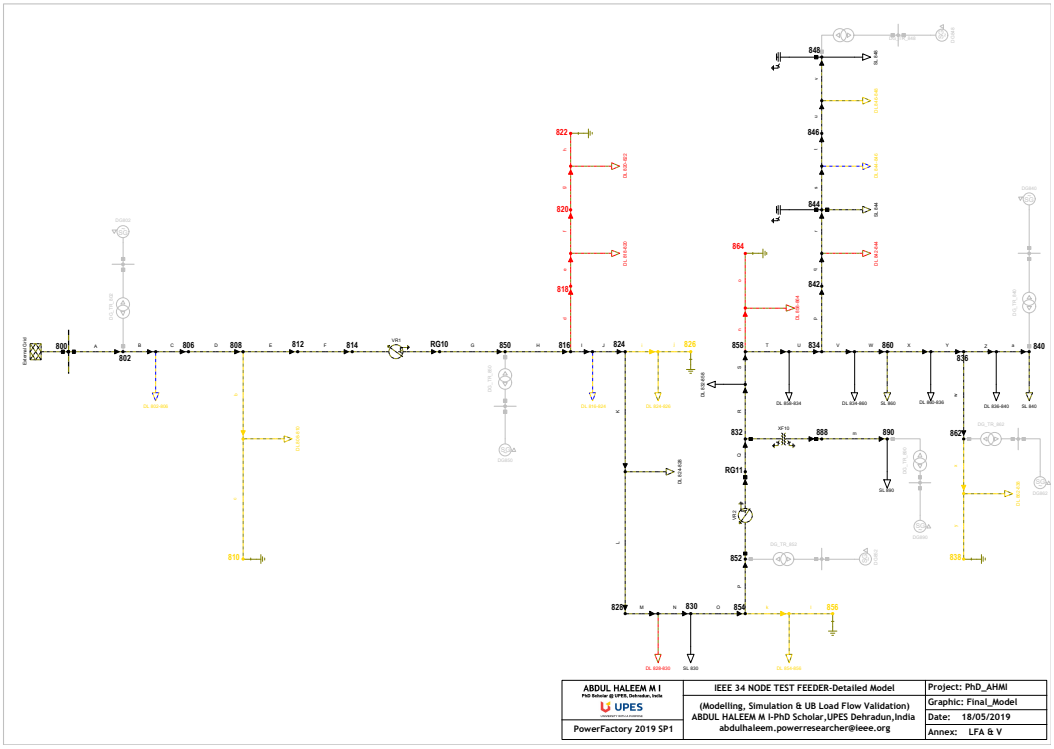

Figure 1. IEEE 34 node feeder modeled in DIgSILENT PowerFactory.

3.2. Load Flow Simulations and Validations

From the provided load and generation data, the load flow algorithms are used to determine the line flows and voltages for a significant power system. It is a crucial and fundamental tool for power system analysis and is utilized during both the operational and planning phases. In systems where unbalances may be disregarded, single-phase power flow methods are typically employed. The three-phase balanced hypothesis, however, is inapplicable to distribution systems. For these situations, a three-phase load flow algorithm with full three-phase models is necessary. Additionally, it is imperative to resolve the load flow problem as fast as possible since several applications, particularly in distribution automation and optimization, call for its solution on a periodic basis [27,28].

In the literature, a number of load flow algorithms specifically created for DN have been put forth. These compositions fall into two different categories. The bus voltages were employed as state variables in the first category [29–32] to resolve the load flow problem. This classification was based on the overall topology of a DN. The Gauss implicit Z-Bus approach is the most well-known load flow mechanism in this area [30,31]. Numerous applications have used this technology, which has been adopted by numerous electricity companies. The Newton–Raphson (NR) algorithm was proposed in [32] and was designed to expedite the three-phase load flow employing the rectangular-form voltages as state variables. Branch voltages are used as state variables in [33] to solve the load flow problem with an innovative quick three-phase load flow method for unbalanced radial distribution systems utilizing the NR algorithm. The load flow calculation method selected in DP is an unbalanced, 3-phase (ABC) NR (current equations), as it best suits the nature and behavior of the network model. The load flow simulation settings used in the DP are shown in Figures A1 and A2 of Appendix B. The load flow simulation results show very close results to the results published by the IEEE PES DSAC [25]. The load flow results from the DP model with node voltages and line section currents along with their angles are given in Appendix A (Tables A2 and A3, respectively).

Tables 1 and 2 show the percentage errors in node voltage and angle following a comparison with published load flow values. Tables 3 and 4 contain a list of the line current magnitude and angle percentage errors. The DP model load flow is converged in three iterations, and the results are shown in Table 5.

Table 1. Line to neutral voltage error deviation from the IEEE published results.

	A-N Voltage *	**B-N Voltage ***	**C-N Voltage ***
Minimum Error	−0.0021	−0.0007	−0.0002
Maximum Error	0.0002	0.0004	0.0006
Average Error	−0.0001	0.0001	0.0000

* per unit.

Table 2. Line-to-neutral angle error deviation from the IEEE published results.

	A-N Angle *	**B-N Angle ***	**C-N Angle ***
Minimum Error	−0.0091	−0.0001	−0.0006
Maximum Error	0.0737	0.0000	0.0000
Average Error	0.0095	0.0000	−0.0001

* degree.

Table 3. Line current error deviation from the IEEE published results.

	Line A *	Line B *	Line C *
Minimum Error	−0.0256	−0.0067	−0.0020
Maximum Error	0.2857	0.0322	0.0285
Average Error	0.0111	0.0020	0.0017

* Ampere (A).

Table 4. Line current angle error deviation from the IEEE published results.

	Line A Current Angle *	Line B Current Angle *	Line C Current Angle *
Minimum Error	−0.0004	−0.0029	−0.0128
Maximum Error	0.0014	0.0004	0.0004
Average Error	0.0000	0.0000	−0.0003

* degree.

Table 5. Load flow results from DP model vs. IEEE published results (in brackets).

	Active Power (kW)	Reactive Power (kVAr)	% Error
Total System Input	2043.13 (2042.872)	290.47 (290.258)	kW = 0.0001 kVAr = 0.0007
Total Load *	1769.66 (1769.824)	1051.47 (1051.547)	kW = 0.0000 kVAr = 0.0000
Total Losses	273.47 (273.049)	35.28 (34.999)	kW = 0.0015 kVAr = 0.0080

* Total Power factor = 0.86 (0.8597).

From the comparison of the load flow analysis results, it is clear that the results exactly match the results provided by the IEEE DSAC report, with very minimal errors.

3.3. µPMU Placement

Traditional PMUs, which are used in transmission networks, are not ideal for radial DN because of their communication limitations and high cost. The introduction of µPMUs with a high reporting rate is suited for DN and may offer real-time synchrophasor data, such as frequency, ROCOF, and voltage phasors. Furthermore, the optimal deployment of µPMUs at smart radial DN buses reduces the economic burden. Only one main condition is taken into consideration while placing the µPMUs in the modeled IEEE 34 DP model. The condition is to achieve total deployment cost minimization while maintaining full system observability so that the generated events can be observed by at least any of the µPMU to have situational awareness of the event. The best solutions are determined using various optimization techniques, and a complete system observability redundancy index (CSORI) and cost index (CI). Maximum system redundancy is ensured by the highest value of CSORI. CI determines the total cost of optimal µPMUs deployment [34]. In order to identify the critical buses where µPMUs should be installed for effective monitoring, a graph-theoretic approach has been used in [35]. A hybrid approach based on a global search algorithm to determine the optimal subset of buses for µPMU placement is proposed in [36]. A heuristic algorithm based on the k-means clustering technique to determine the optimal placement of PMUs is proposed in [37]. All these investigations (Table 6) show that the test feeder can have 12 optimal locations for cost-effective installations, maintaining full system observability. Out of the two combinations of the 12 µPMU locations, the one with node 850 is considered instead of node 814, as node 850 is a DG connection node, and the downstream node with lateral tappings can be observed; additionally, the regulator (RG10) output parameters need to be monitored, rather than the regulator input parameters, to set the desired tap positions in case the DGs are not integrated. The locations of µPMUs are selected by carrying out a simulation study such that the planned realistic events can be observed by the node voltages and line currents reported by these µPMUs.

Table 6. Investigations on optimal μPMU placements in IEEE 34 node feeder.

Method	Approach	No. of μPMUs	Optimal Locations
[34]	Deployment cost minimization	12	802, 810, 814, 820, 824, 834, 838, 840, 846, 854, 864, and 888
	Full system observability	12 *	802, 808, 820, 824, 834, 836, 846, 850, 854, 858, 862, and 888
[35]	Full system observability	12	802, 808, 814, 820, 824, 834, 836, 846, 854, 858, 862, and 888
	Full system observability	12 *	802, 808, 850, 820, 824, 834, 836, 846, 854, 858, 862, and 888
[36]	Full system observability (with Min. No. of μPMUs)	12	802, 808, 814, 820, 824, 834, 836, 846, 854, 858, 862, and 888
	Full system observability (with Min. No. of μPMUs)	12 *	802, 808, 850, 820, 824, 834, 836, 846, 854, 858, 862, and 888
[37]	Full system observability	12	802, 808, 814, 820, 824, 834, 836, 846, 854, 858, 862, and 888

* Optimal locations selected for data generation.

The DP does not have a μPMU component in the toolbox, but the features of the μPMU can be created as output while generating the output data of the nodes and line sections, such as the magnitude of the voltage, current, and their angles, frequency, etc. This data-generation study focused on the magnitude of μPMU node voltages and line currents and angles. These parameters will be collected from the 12 optimally placed μPMUs in the feeder as shown in Figure 2. Out of the 12 μPMUs, 11 are three-phase μPMUs and one is a single-phase μPMU.

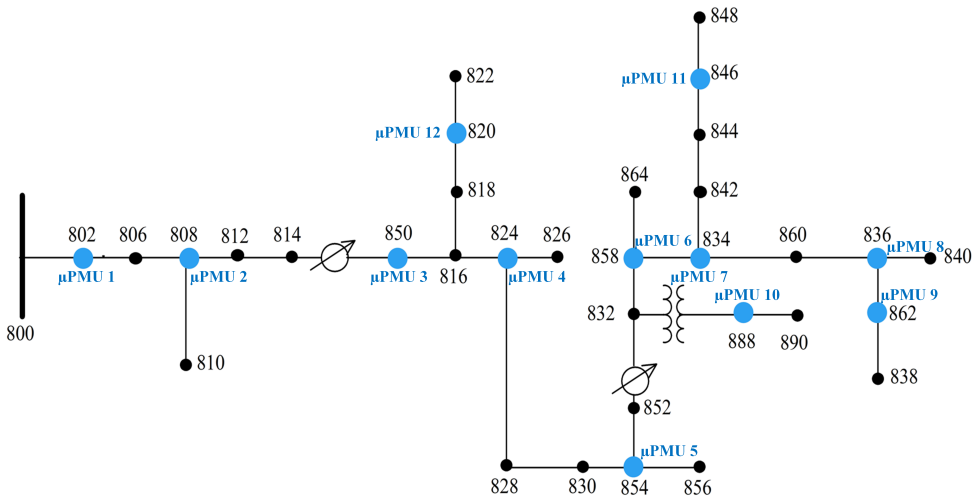

Figure 2. Optimal μPMU locations in the test feeder.

3.4. Sizing and Placement of DGs

There are many different sorts of DGs, from conventional to renewable; however, this study is not specifically focused on any one kind of DG source. The main goal of this effort is to integrate DGs at various places in order to recognize and record their influence during various real-time occurrences using μPMU data. Each DG was modeled as a synchronous generator. The power levels utilized for a DG intended to supply 20% of the test feeder load, and the DG modeling parameters displayed in Table 7 were acquired from [38]. The parameters that were not listed adhered to the DP defaults.

Table 7. DG modeling parameters [38].

V_{rated} = 480 (V)	kVA_{rated} = 410 (kVA)	P_{rated} = 350 (kW)
V_{Sched} = 1 (p.u.)	Q_{max} = 0.5 (p.u.)	Q_{min} = −0.25 (p.u.)
pf = 0.8536585	X_d = 1.76 (p.u.)	X_q = 1.66 (p.u.)
$X_{d'}$ = 0.21 (p.u.)	$X_{q'}$ = 0.18 (p.u.)	$X_{d''}$ = 0.13 (p.u.)
$X_{q''}$ = 0.11 (p.u.)	r_a = 0 (p.u.)	r = 0 (p.u.)
r_{1r} = 0 (p.u.)	X_{1r} = 0 (p.u.)	X_0 = 0 (p.u.)

To link the DGs to the nodes, a 500 kVA transformer in a delta–delta arrangement was used. The 500 kVA line transformer utilized in the selected feeder served as the basis for the modeling parameters for these transformers. DGs were only installed on the three-phase nodes and the three-phase radial tappings or laterals because only three-phase DGs were used. With the exception of the substation and the voltage regulators, radial tapping from 832 is the only area of the circuit that operates at the 4.16 kV level. It also houses the circuit's line transformer. The only capacitors in the circuit are located at 844 and 848 on radial tapping from 834. There were numerous DG places that were feasible. The modifications tried were on the radial tapping points as well as the main feeder, close to and distant from the substation, close to the voltage regulators. The connection nodes 802, 840, 848, 850, 852, 862, and 890 were specifically evaluated. Each DG was built with a default size of 20% of the original feeder load, resulting in a 410 kVA unit with a 350 kW planned real-power output. The study's focus is on the use of DGs at various feeder locations to produce data for various real-time occurrences and their classes.

3.5. µPMU-Based Real-Time Event Data Generation

At a 120 Hz sampling rate (or one sample every 0.008333 s), the optimally placed µPMUs record 4 fundamental measurements on 3 phases, for a total of 12 measurement channels: voltage magnitude, current magnitude, voltage phase angle and current phase angle. This paper generates 30 min of µPMU data considering the planned and unplanned outage events in the real rural overhead DN. The author defines a total of 109 real-time events from his real grid operation experience. This includes 62 planned and 47 unplanned network events. The 12 µPMUs measure and report 16,848,000 data points in 30 min.

3.5.1. Realistic Real-Time Events

The unbalanced overhead DN has quite a lot of real-time events, as it is inherent in nature with many complexities to be addressed. The idea behind selecting an unbalanced overhead DN is to incorporate all the relevant real-time events that happen in the network. The events range from planned to unplanned events. Even though most of the events can fall into both categories, the events that are created by the triggering of protection devices are considered unplanned, and all the scheduled events are considered as planned events. To keep the events more realistic, almost all the event types are included, covering different components and locations in the test feeder. A total of 109 realistic events were generated using the test feeder model as listed in Table A4 of Appendix A. The events include capacitor bank switching, circuit breaker (CB) switching, CB trip, DG switching, DG trip, line de-energization, line energization, load switching, load trip, overhead line (OHL) jumper events, faults events, temporary faults, tap-changer events, transformer outage and energization, transformer trip, fault-clearing events and low-voltage complaints from customers.

3.5.2. Data-Generation Settings in DP

The chosen test feeder is flawlessly modeled in DP and is absolutely required for the data generated. The events are defined in relation to the chosen DN model elements. To categorize the events as switching, fault, or fault-clearing events, specific components are chosen. The features include a variety of execution time options in hour, minute, and second formats, as well as options for modifying the phase type individually. Moreover, they enable the usage of various fault classes, impedance levels, and the percentage of fault

location distance in the line section. In order for the generated data resolution to match that of the actual data supplied by the PMU, the data-generation settings must be chosen with extreme care. With the DP settings listed below, the RMS simulation is run with all of the simulation occurrences. For the unbalanced, three-phase ABC system, RMS values (electrical and mechanical transients) with a step size of 0.008333 are chosen as the default initial condition settings (120 measurements per second). The default values are chosen for all other simulation settings. The main simulation settings used in the DP for the data generation are shown in Figures A3–A6 of Appendix B.

3.5.3. Event Simulations and Plots

By choosing the relevant component in the model and providing the type of event, execution time, selected element action, phases impacted, % of line section fault location, fault type, impedance, and other parameters, 109 intended events are simulated. If any adjustments to the simulation settings are required, the list of simulation events can be further changed.

Twelve μPMUs were already installed at the optimal nodes; hence, the focus of this study is exclusively on measuring them. The study only considers the node voltage (line-to-neutral) and the line currents, despite the fact that PMU devices can monitor a wide range of properties. The data-production criteria were designed to take into consideration these data for future work on event detection, categorization, and section identification. The unbalanced loading on the test feeder, which comprises a number of single-phase to-neutral and two-phase to-neutral loads, is what causes the phase-to-neutral voltage to be measured. The two fundamental graphs generated for each PMU are phase current vs. time and node voltage (phase to neutral) vs. time.

4. Results

The plots shown here for each different event are the most impacted μPMUs in the network with respect to that particular event. Plots are in per-unit values of the line-to-neutral voltage and line currents of the relevant μPMUs over the time in seconds. The results demonstrate that when the capacitor bank is switched on, the voltage magnitude increases to compensate for the reactive power and decreases when it is switched off. The line currents that the upstream (US) and downstream (DS) μPMUs report are dependent on the initial switching conditions. For both capacitor switch-on and switch-off events, line current undershoots and overshoots are observed.

Line voltages drop to zero during main CB tripping occurrences, while line currents drop to zero following a switching spike, depending on the reason of the tripping. In the event of a failure, the voltage on the affected line or lines will drop to zero, while the current will rise to the fault level and remain there until the circuit breaker trips. When the CB closes, the voltage rises from zero to the nominal network voltage, and the current shoots up to the maximum current before settling back to the usual load current value after a few seconds. The results of DG switch-on events show a drop in line voltages and a rise in line currents, but both values return to normal after a few seconds, whereas the DG switch-on event indicates a voltage and current increase in the nearest μPMU and a voltage rise and current drop in the farthest μPMU. Similarly, all the key real-time events in an unbalanced DN selected for this study, along with their impact on the node voltages and line currents from the relevant μPMUs, are observed as listed in Table 8.

The realistic data created for numerous real grid events demonstrate how applicable they are in a wide range of use cases, including real-time μPMU data-based predictive maintenance of key assets (transformers, OHLs, CBs, DGs, etc.). The dynamics reported by μPMUs help with real-time asset health monitoring and aging analysis. Apart from these applications, the data can be further used to conduct offline analytics for network planning, scheduled maintenance, topology modifications, etc.

Table 8. Event category chart and their plots.

Sl. No.	Event Description	Figure Numbers
1	Capacitor Bank Switching	Figures 3–6
2	Circuit Breaker Trip	Figures 7 and 8
3	Circuit Breaker Switching	Figures 9 and 10
4	DG Switching	Figures 11–14
5	DG Trip	Figures 15 and 16
6	Line De-energization	Figures 17 and 18
7	Line Energization	Figures 19 and 20
8	Load switching	Figures 21–24
9	Load trip Event	Figures 25 and 26
10	Open Circuit Fault	Figures 27 and 28
11	Short Circuit Fault	Figures 29 and 30
12	Tap Changer	Figures 31–34
13	Temporary Fault	Figures 35 and 36
14	Transformer Outage	Figures 37 and 38
15	Transformer Energization	Figures 39 and 40
16	Transformer trip	Figures 41 and 42
17	Off Supply Complaint	Figures 43 and 44
18	Unbalance Voltage Complaint	Figures 45 and 46

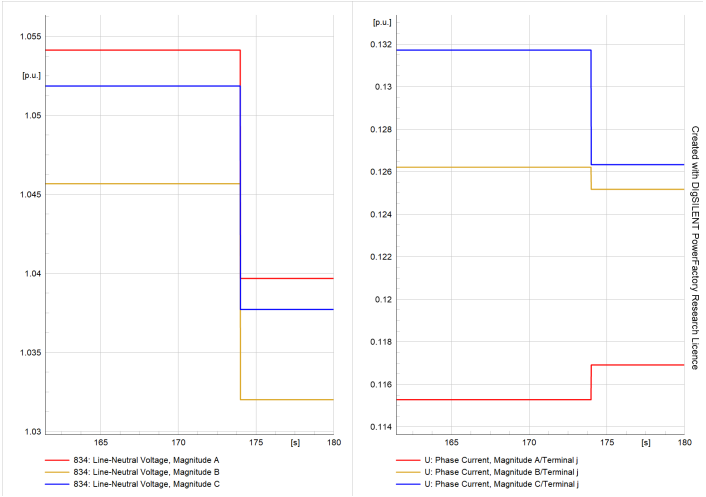

Figure 3. Capacitor bank switch-off event (μPMU7).

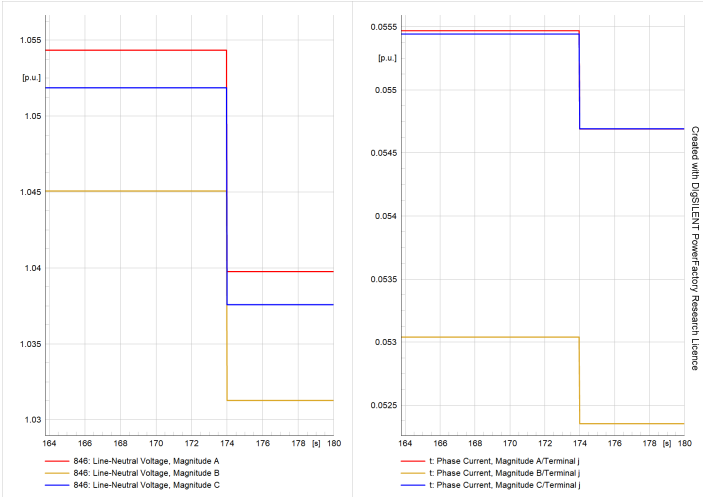

Figure 4. Capacitor bank switch-off event (μPMU11).

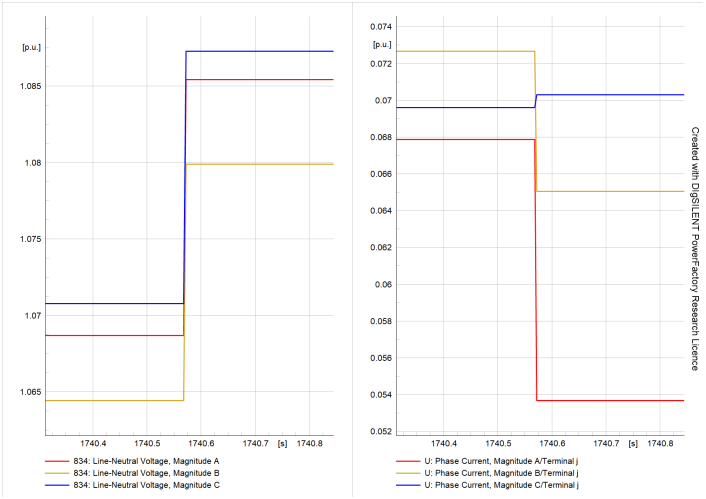

Figure 5. Capacitor bank switch-on event (µPMU7).

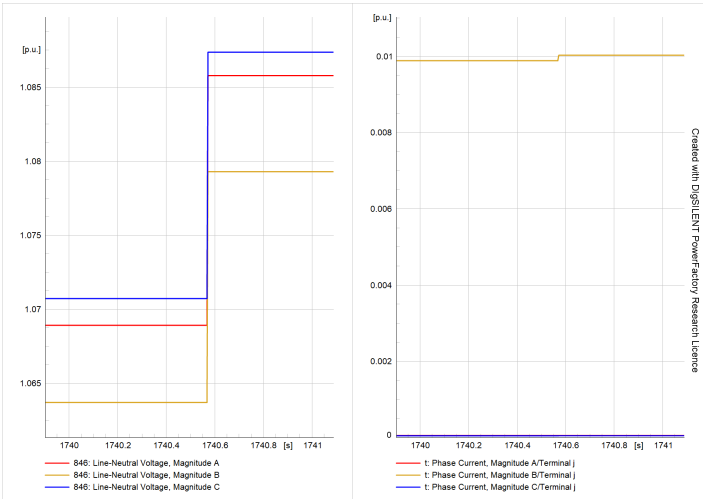

Figure 6. Capacitor bank switch-on event (µPMU11).

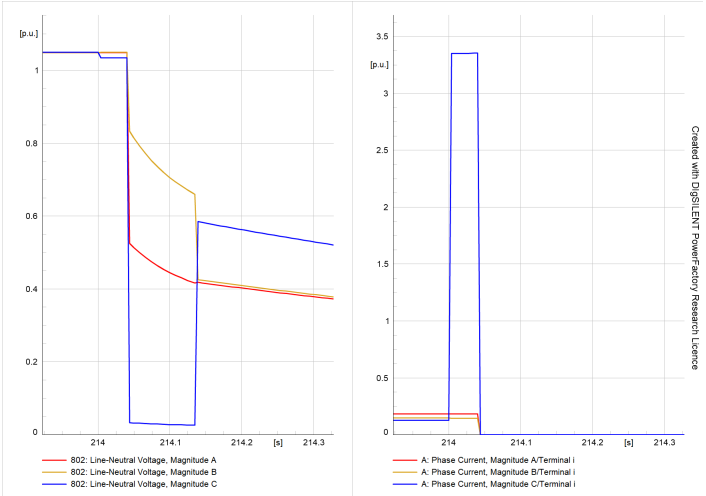

Figure 7. CB trip event (µPMU1).

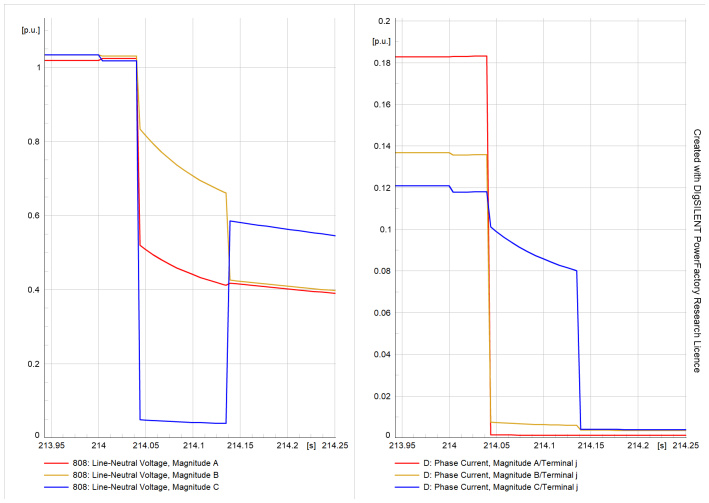

Figure 8. CB trip event (μPMU2).

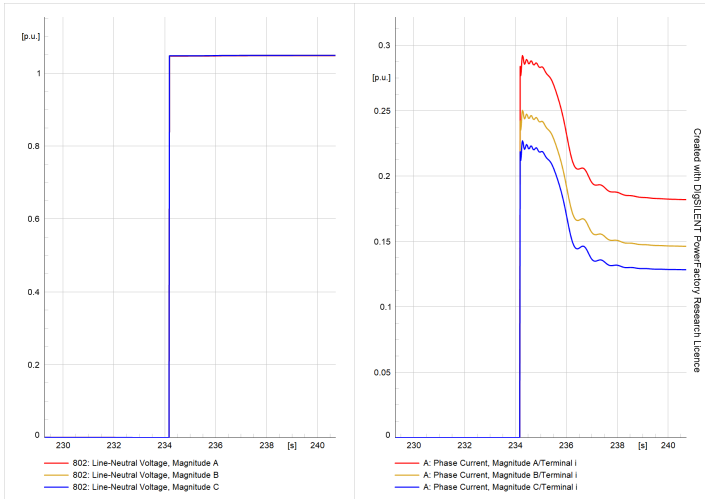

Figure 9. CB close event (μPMU1).

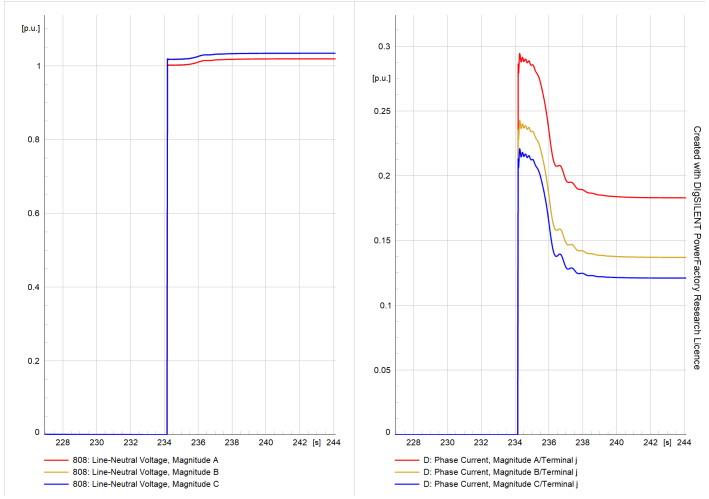

Figure 10. CB close event (μPMU2).

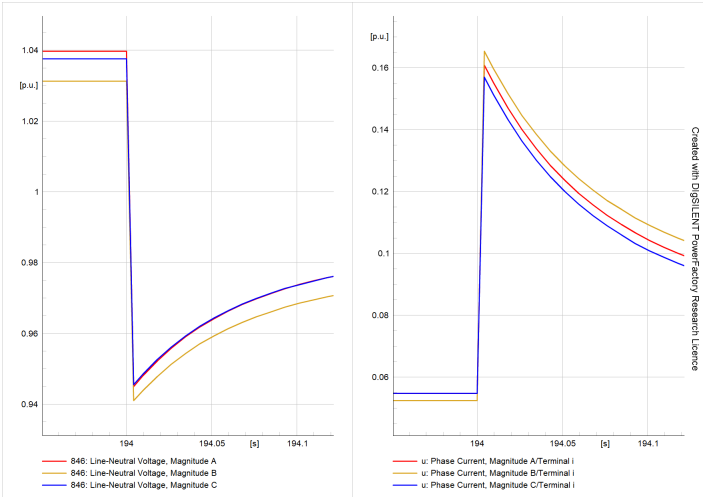

Figure 11. DG switch-on event (µPMU11).

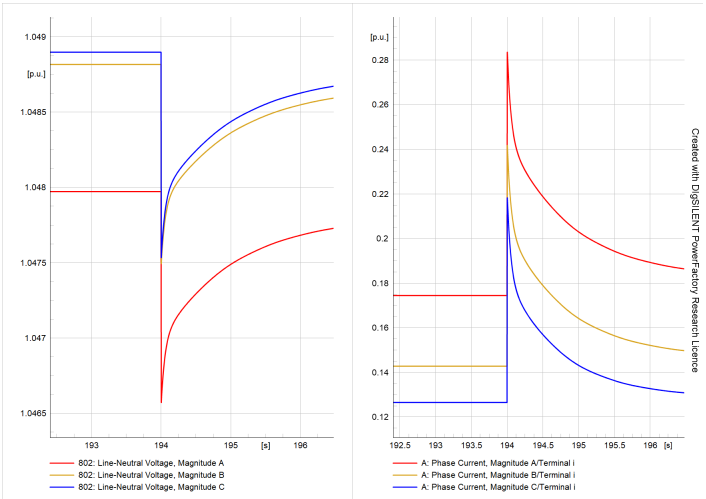

Figure 12. DG switch-on event (µPMU1).

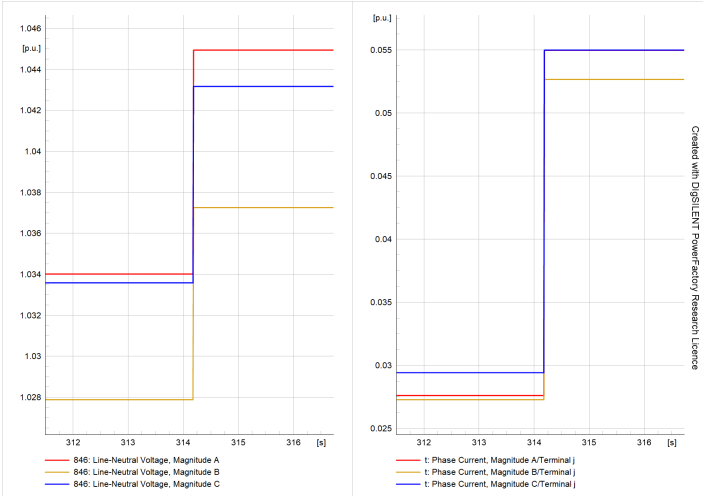

Figure 13. DG switch-off event (µPMU11).

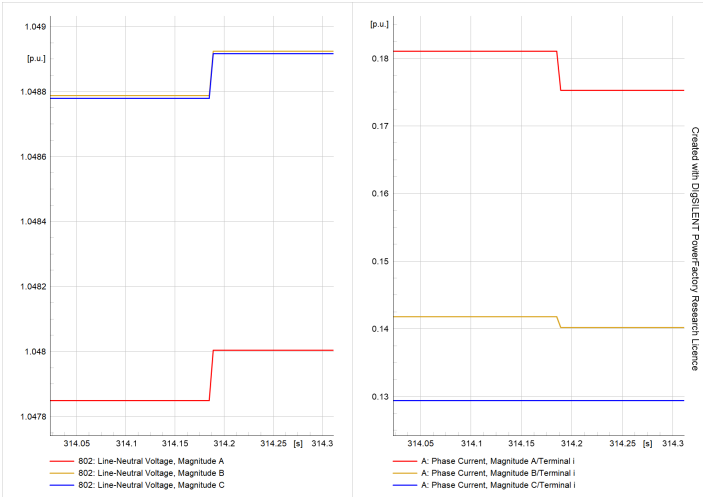

Figure 14. DG switch-off event (µPMU1).

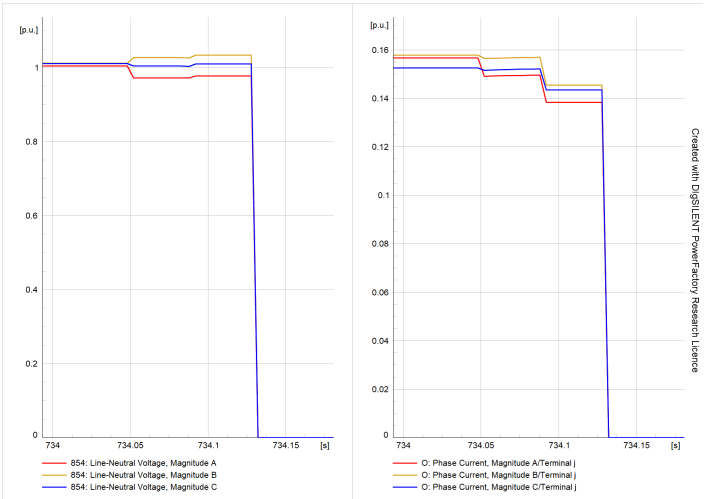

Figure 15. DG trip event (µPMU5).

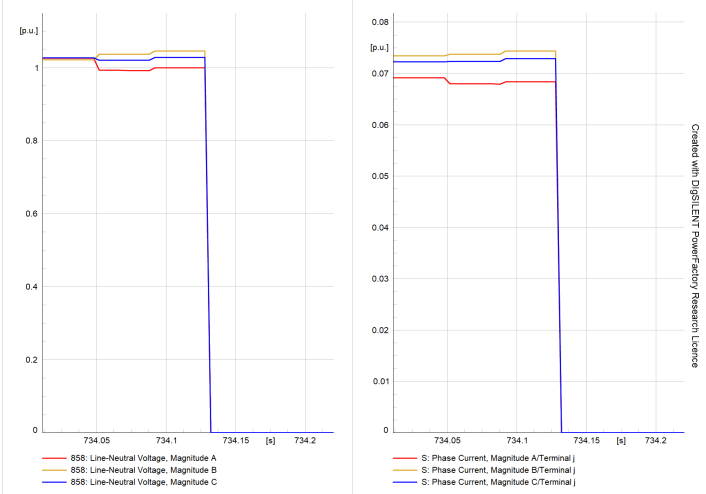

Figure 16. DG trip event (µPMU6).

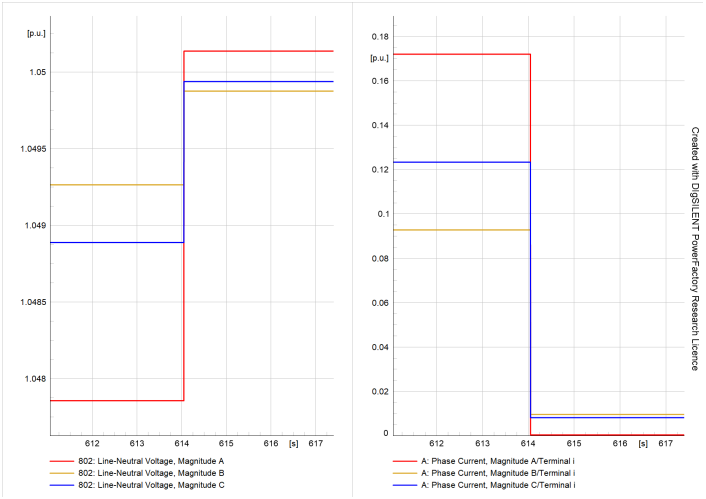

Figure 17. Line section de-energization (µPMU1).

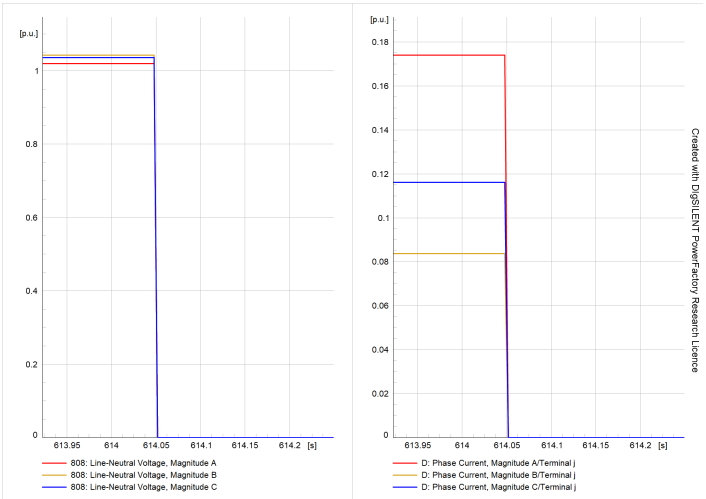

Figure 18. Line section de-energization (µPMU2).

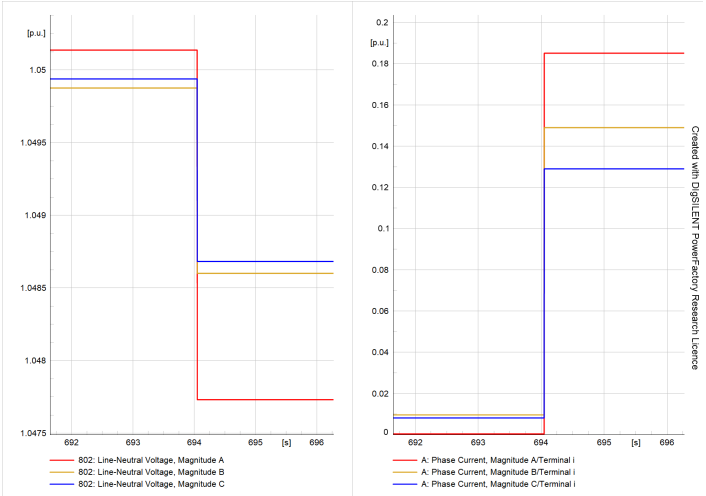

Figure 19. Line section energization (µPMU1).

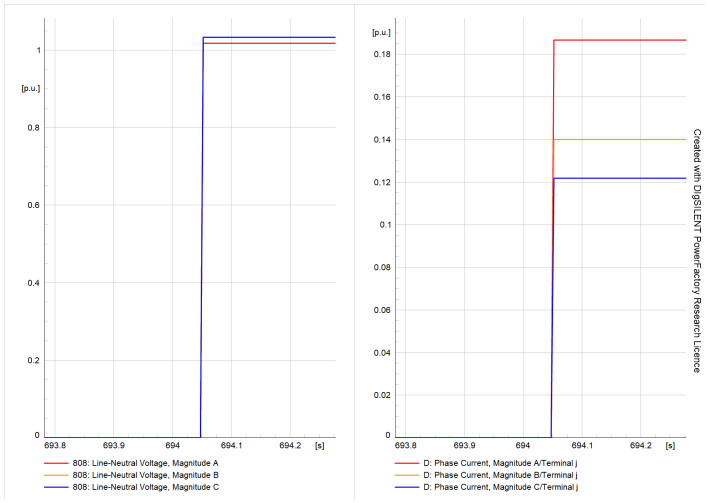

Figure 20. Line section energization (µPMU2).

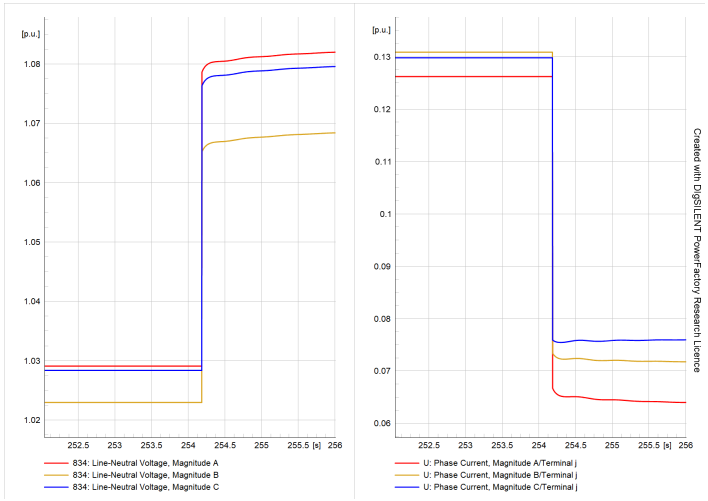

Figure 21. ABCN load switch-off event (µPMU7).

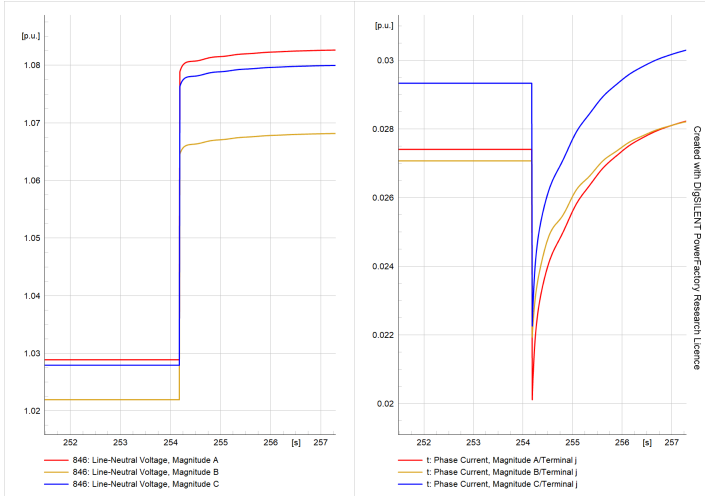

Figure 22. ABCN load switch-off event (µPMU11).

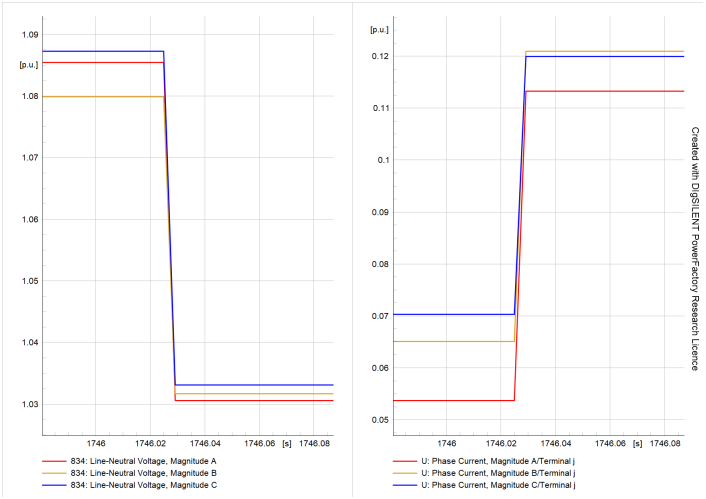

Figure 23. ABCN load switch-on event (µPMU7).

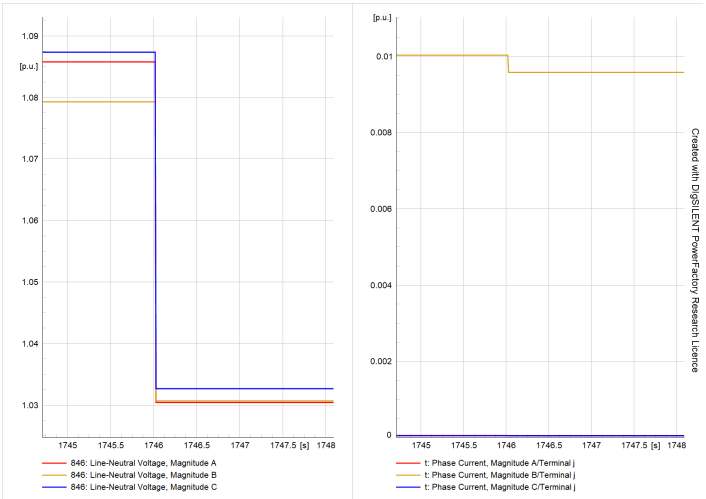

Figure 24. ABCN load switch-on event (µPMU11).

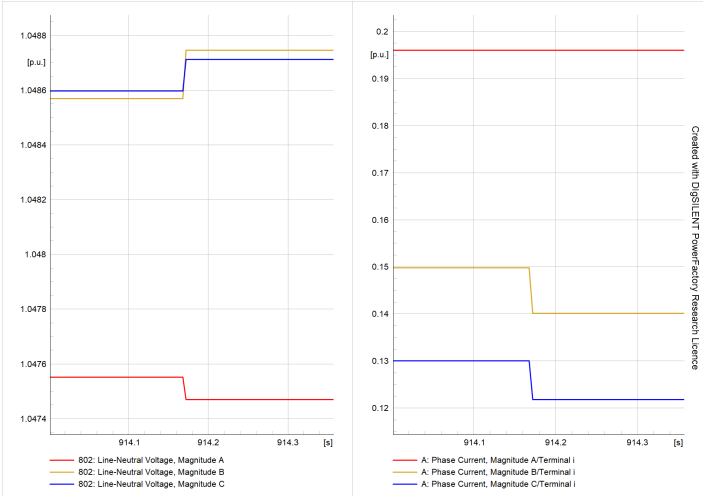

Figure 25. BCN load trip event (µPMU1).

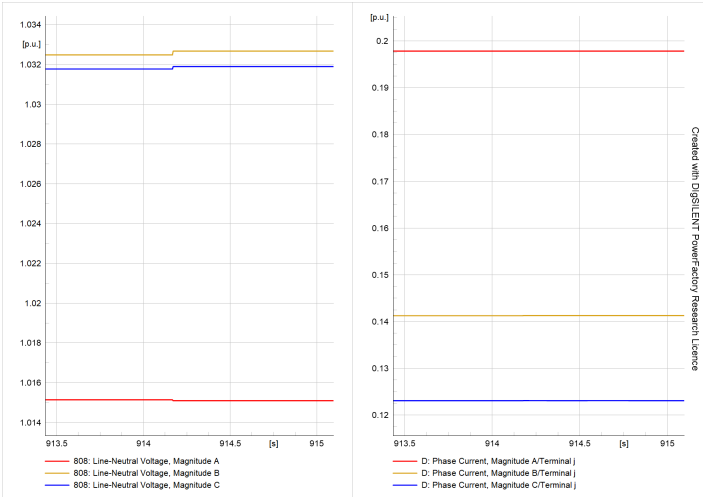

Figure 26. BCN load Trip Event (µPMU2).

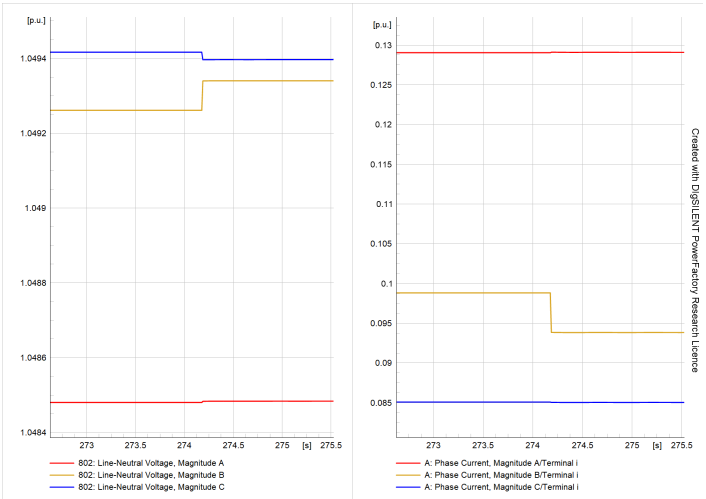

Figure 27. B-N jumper parted open circuit fault (µPMU1).

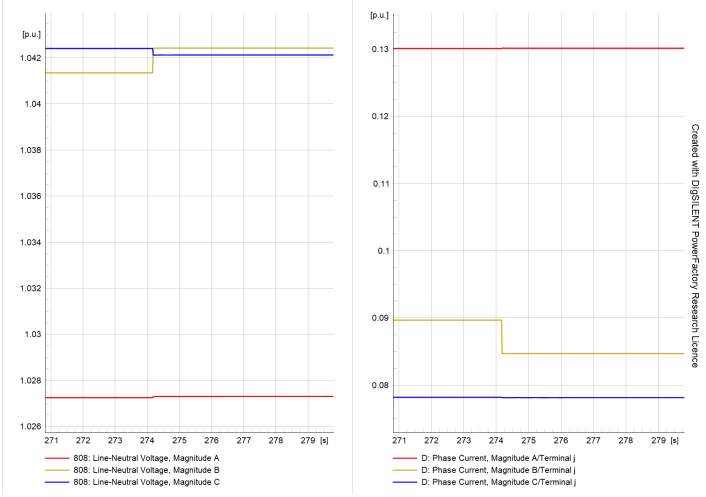

Figure 28. B-N jumper parted open circuit fault (µPMU2).

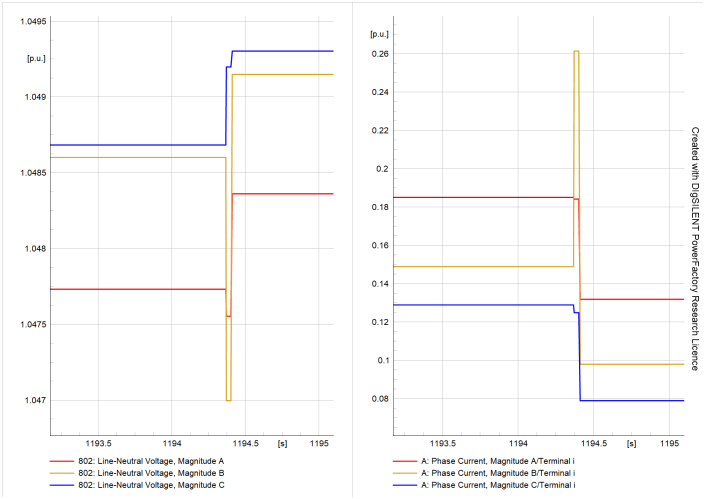

Figure 29. BG fault event (µPMU1).

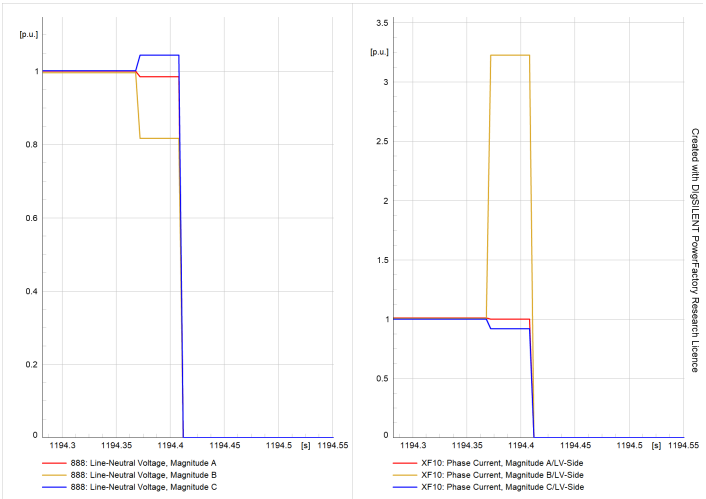

Figure 30. BG fault event (µPMU2).

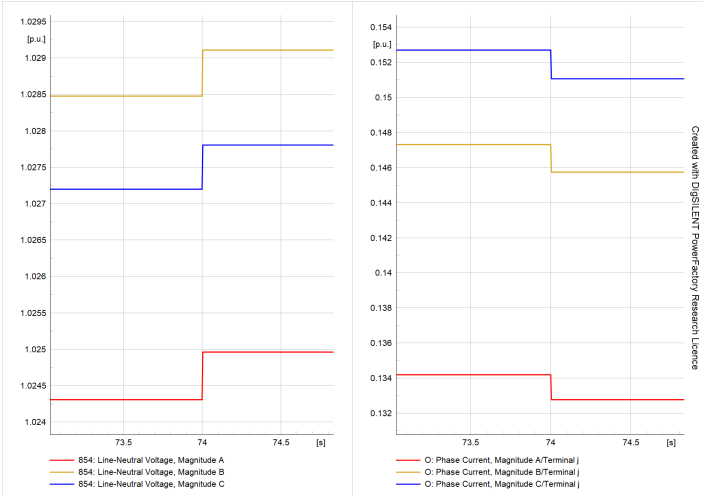

Figure 31. Tap lowering (µPMU5).

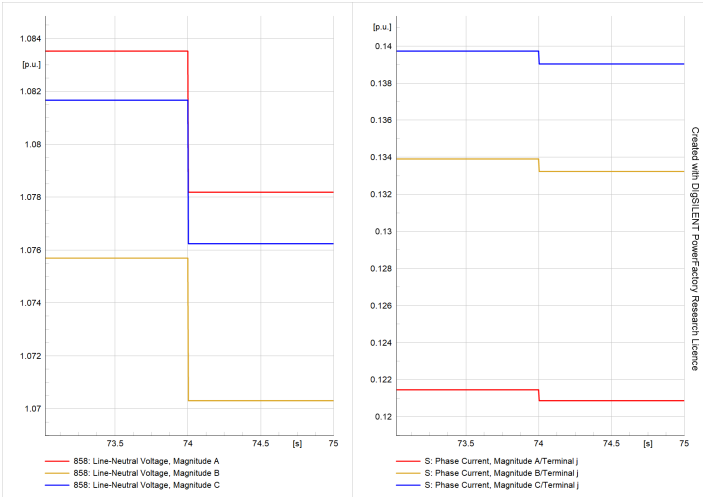

Figure 32. Tap lowering (µPMU6).

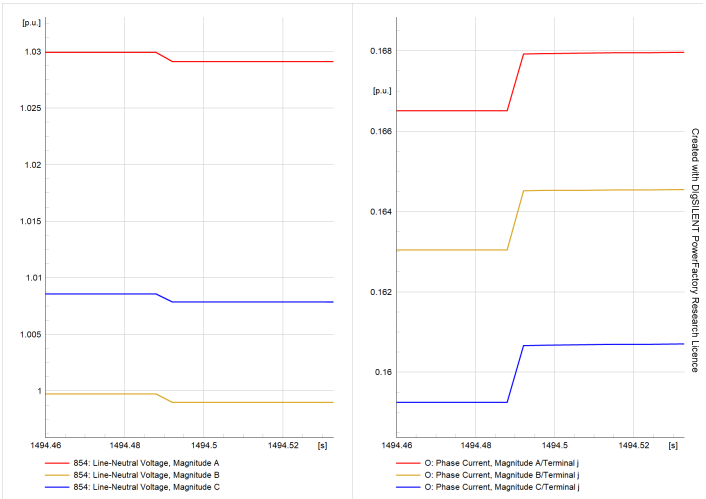

Figure 33. Tap Raising (µPMU5).

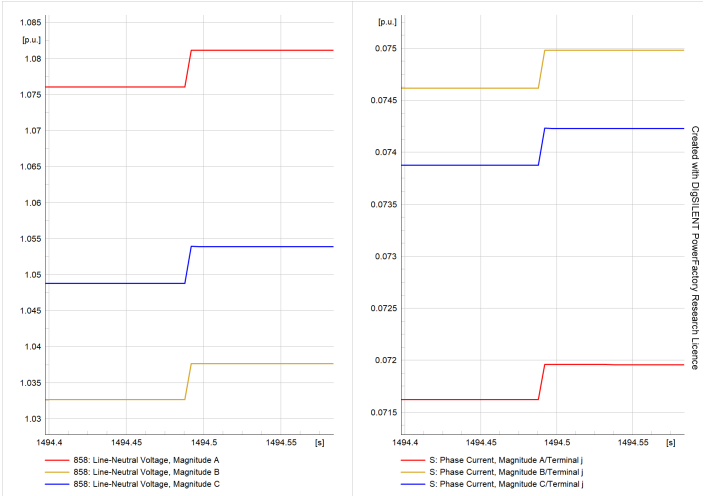

Figure 34. Tap raising (µPMU6).

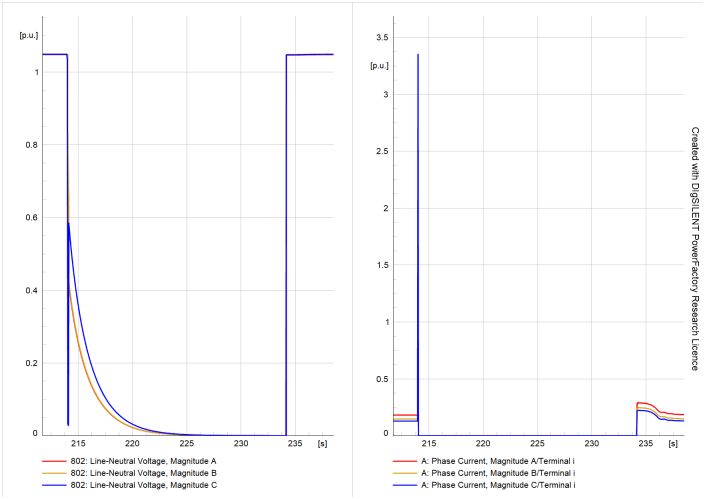

Figure 35. Temporary fault and reclosing (µPMU1).

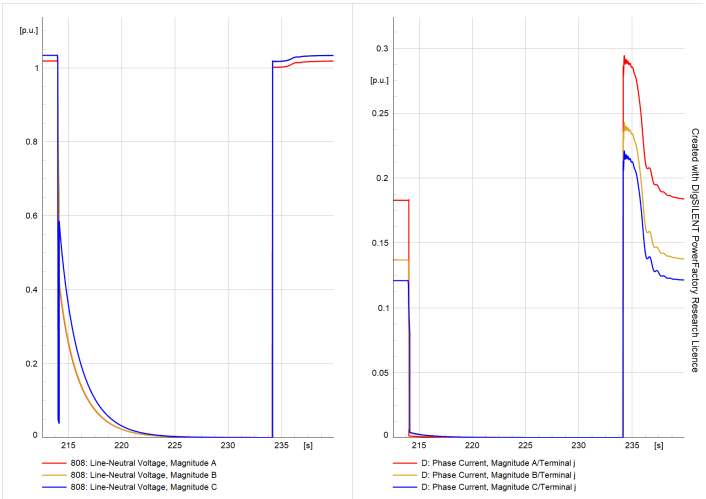

Figure 36. Temporary fault and reclosing (µPMU2).

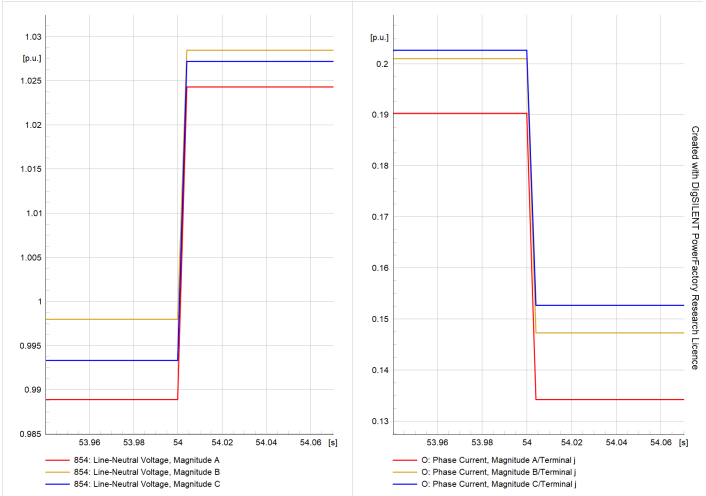

Figure 37. Transformer outage (µPMU5).

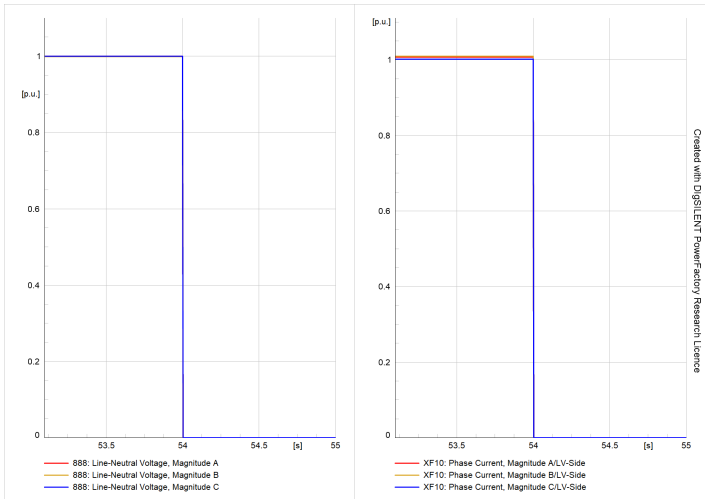

Figure 38. Transformer outage (µPMU10).

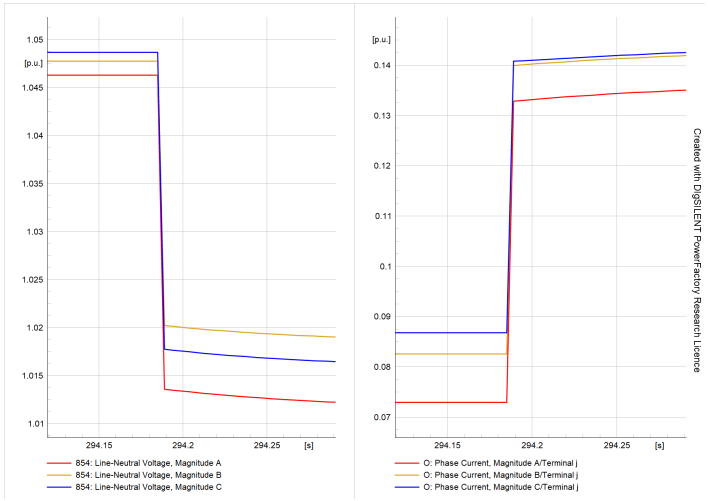

Figure 39. Transformer energization (µPMU5).

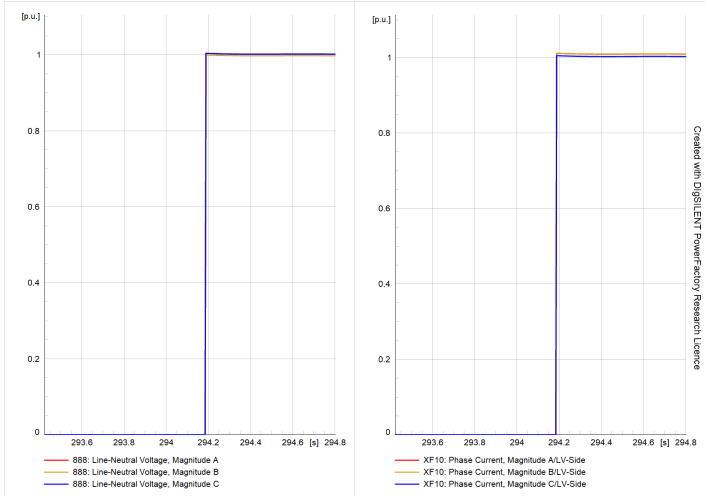

Figure 40. Transformer energization (µPMU10).

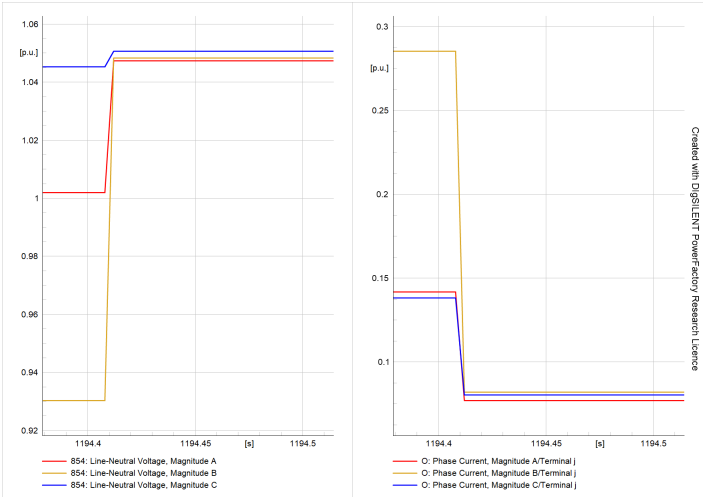

Figure 41. Transformer trip (μPMU5).

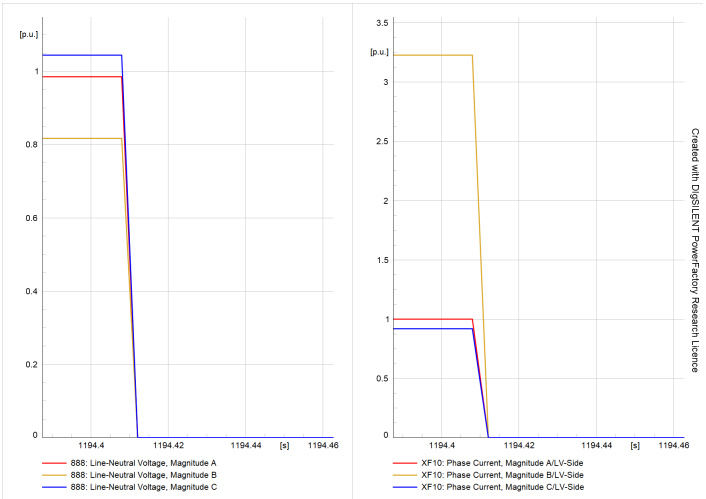

Figure 42. Transformer trip (μPMU10).

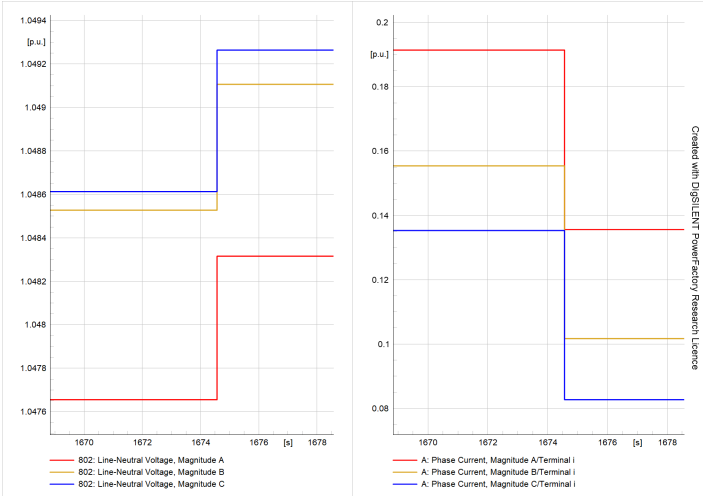

Figure 43. Off supply complaint (μPMU1).

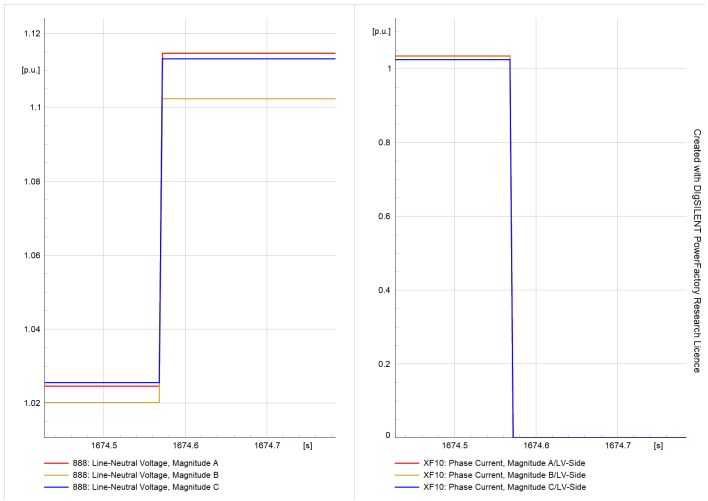

Figure 44. Off supply complaint (µPMU10).

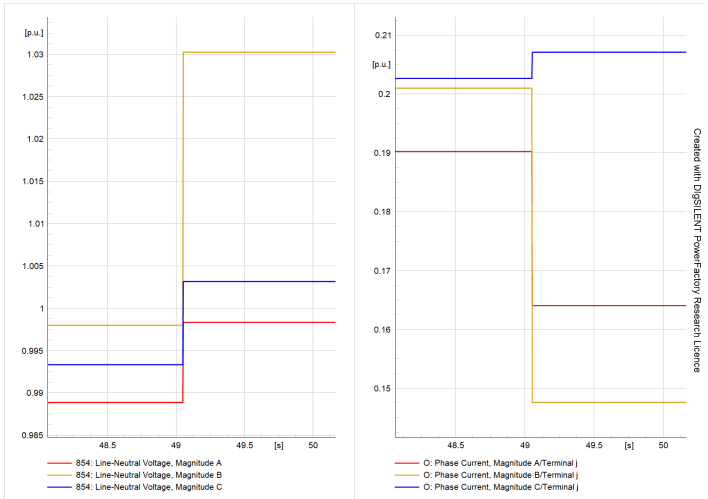

Figure 45. Unbalance voltage complaint (µPMU5).

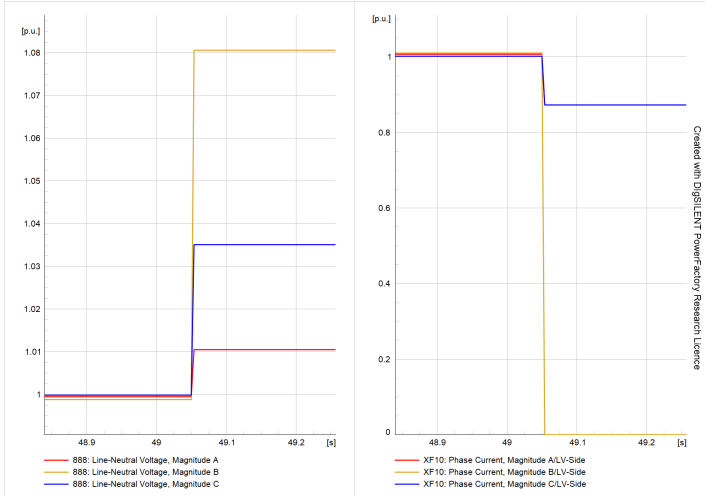

Figure 46. Unbalance voltage complaint (µPMU10).

5. Data Validation

Validation of the results obtained for the various real-time events was performed using published real data from the real DN. The generated data are based on a number of planned normal and abnormal events to observe and understand the dynamics created by them,

whereas the real-time network data observed by the real µPMUs are capable of capturing all the grid dynamics over time. Because the event characteristics are solely determined by the network's initial conditions and other inherent characteristics, the validation focuses on the main parameter features of the individual events, such as node voltage and line currents and their variations.

The generated µPMU data for real-time events, such as capacitor bank switching, fault, CB trip, open, reclosing, and DG switching, were validated by comparing them to the published real data. All other events were validated using the load flow variations at the respective nodes, as the real-time data for these events are unavailable in the literature.

5.1. Capacitor Bank Switching

Capacitor-bank-switching events refer to the switching on or off of capacitor banks in power systems. These events can cause transient and voltage disturbances, which can lead to equipment damage or system failure. Therefore, it is important to detect and monitor these events in real time. This can be achieved using a combination of current and voltage sensors equipped with the µPMUs installed in the DN. The sensors measure the current and voltage signals, which are then processed to detect the capacitor-switching events.

5.1.1. Capacitor Bank Switch-Off Event

When the capacitor bank was kept off, all of the three-phase voltages dropped from their initial values, but all of the variations were within the defined limits. During this event, there was a rise in the R-phase current, no noticeable variation in the Y-phase current, and a drop in the B-phase current. The voltage and current variations shown in the generated data (Figures 47 and 48) were compared and validated with the real µPMU data observed during the capacitor bank switch-off event (Figure 49) published in [15].

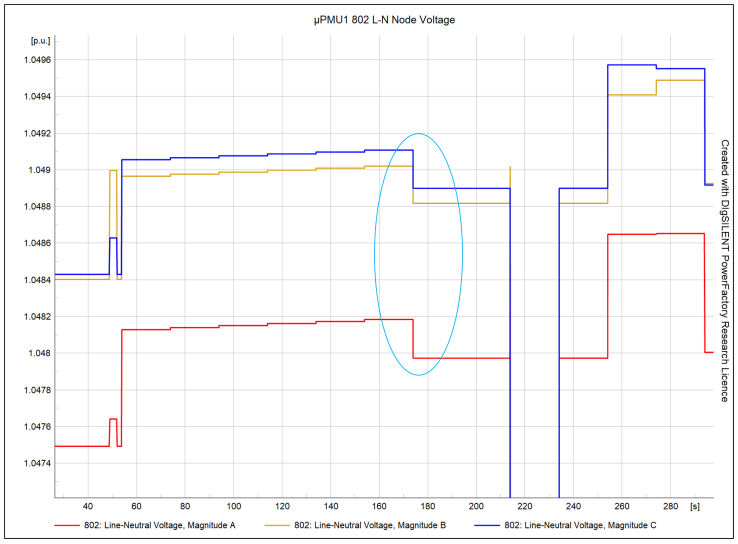

Figure 47. Capacitor bank switch-off event (voltage variations).

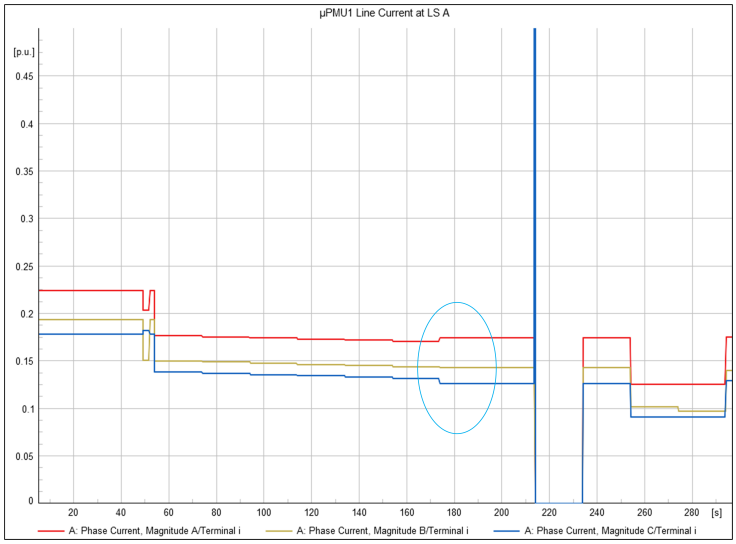

Figure 48. Capacitor bank switch-off event (current variations).

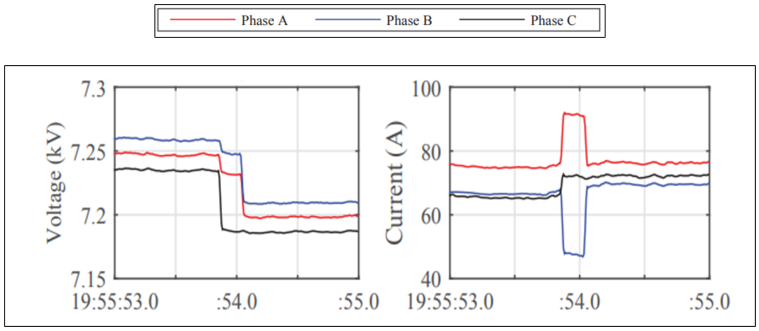

Figure 49. Capacitor bank switch-off event: voltage and current variations validation using real µPMU data [15].

5.1.2. Capacitor Bank Switch-On Event

The voltage and current fluctuations of the generated data (Figures 50 and 51) are as expected. The node voltage at all the phases was raised due to the capacitor bank switch-on event, and consequently, there was a reduction in the line currents at each phase. The same scenario was compared and validated against the actual µPMU data (Figure 52) provided in [15].

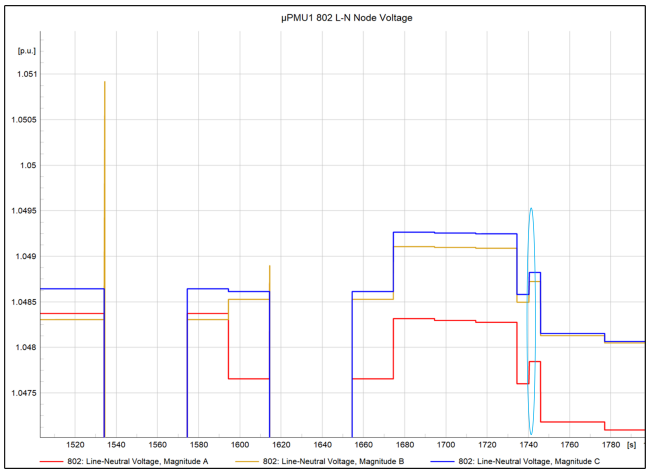

Figure 50. Capacitor bank switch-on event (voltage magnitude).

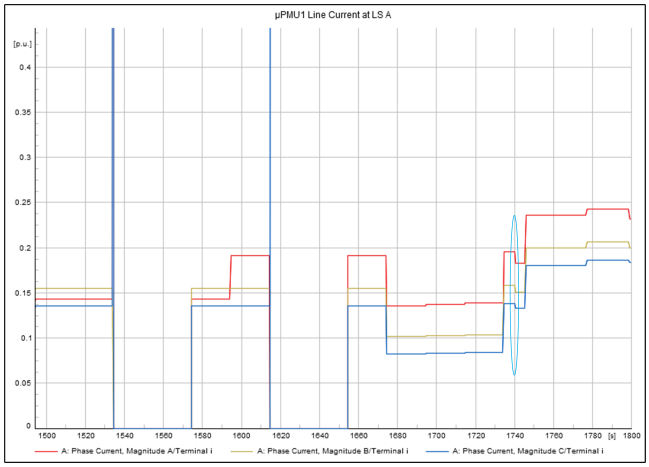

Figure 51. Capacitor bank switch-on event (current magnitude).

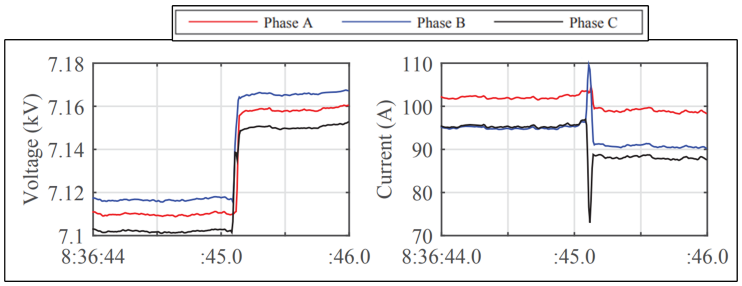

Figure 52. Capacitor bank switch-on event (voltage and current magnitude) validation using real µPMU data [15].

The three-phase capacitor bank switching study shows that the transient currents during the switching events depend on the initial conditions, with the possibility of a rise and drop in the current values. The system is considered normal until the parameter studies are within the limits.

5.2. Fault, Trip, CB Open, and Reclose Events

The generated event data for the fault, trip, CB open, and reclose events observed by the upstream and downstream µPMUs are shown in Figures 53 and 54. These results are based on a B-phase-to-ground fault generated using the modeled network. The real data available in [10] are for a B-phase-to-neutral fault, but if the neutral wire in a three-phase distribution system is solidly grounded, a phase-to-neutral fault can be considered a type of phase-to-ground fault. This is because in a solidly grounded system, the neutral is connected directly to the earth, which means that any fault on the neutral wire will cause a current to flow directly to the ground. As a result, the fault can be considered a phase-to-ground fault, even though it originated on the neutral wire [39]. For validation, these events were compared with the published real data, adapting the relay settings from [10] as shown in Figure 55.

As soon as the fault occurs, the upstream µPMU shows a considerable drop in the voltage and a rise in the current of the B-phase, with minor changes in other phases. After the breaker trip event, almost all the phase voltages show similar values, but all the phase current values reach near zero. When CB completely opens, all the phase voltages reach the limits of their normal values, and the three-phase currents drop to zero. After the reclose event, all the node voltage and the line currents return to their pre-fault normal values as the breaker gets closed, and the loads are immediately connected. This means that the fault was temporary, and the closing of the CB will ensure the healthiness of the network and components.

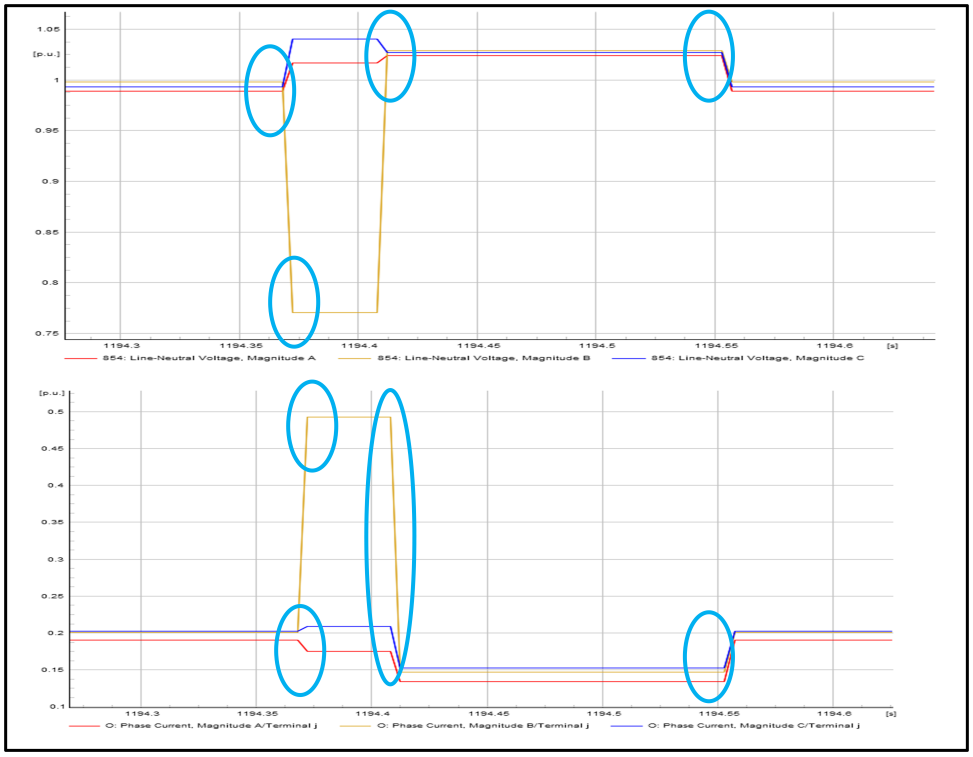

Figure 53. B-G fault, trip, CB open, and reclose events observed upstream.

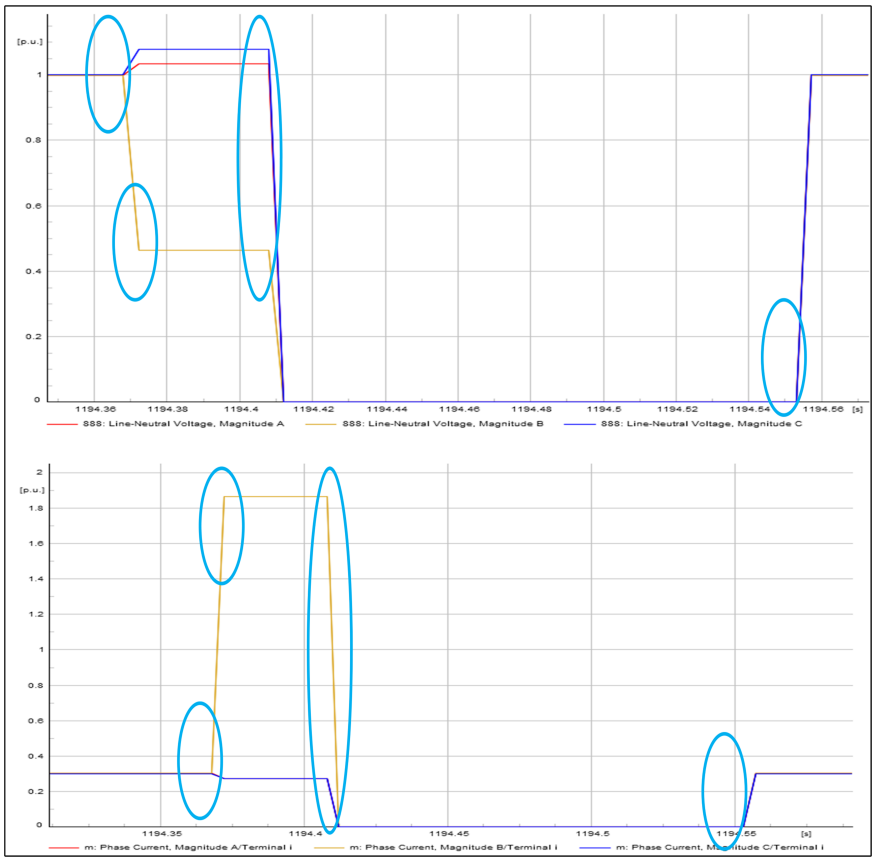

Figure 54. B-G fault, trip, CB open, and reclose events observed downstream.

The fault and trip events observed by the downstream μPMU are more or less the same dynamics observed by the upstream μPMU, but right after the CB opening event,

both voltage and current values of the phases drop to zero. The reclose event observed by this μPMU is similar to the normal pre-fault values of the voltages and currents.

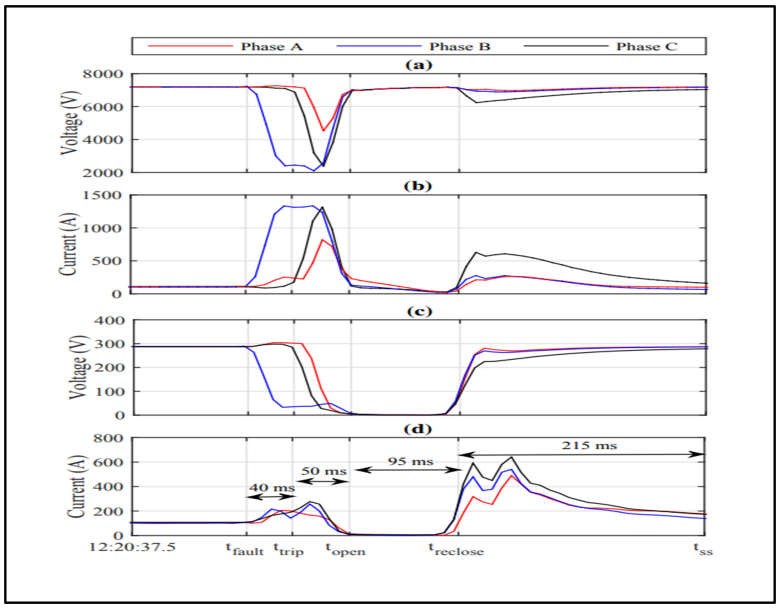

Figure 55. B-G fault, trip, CB open, and reclose events observed at upstream (**a**,**b**) and downstream (**c**,**d**) (voltage and current magnitude) [10].

The generated fault event results are comparable with the dynamics of the fault occurrence process and reclose events presented in [10].

5.3. DG-Switching Event

The event considered for validation is the DG switch-on event, as the real data available in the literature are for this event. Soon after the DG is switched on, the node voltage per phase drops a little bit from the initial conditions and settles down to a comparatively lower value than the initial values per phase, whereas the currents overshoot to a high value and settle down to a slightly higher value than the initial line current magnitude. The generated DG-switching event in Figure 56 is validated using the DG-switching event captured in [40]. The real μPMU observations are shown in Figure 57. The results are more or less close to the published real μPMU values.

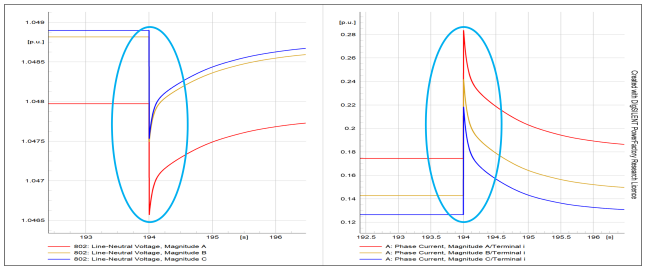

Figure 56. DG-switching event (voltage and current variations).

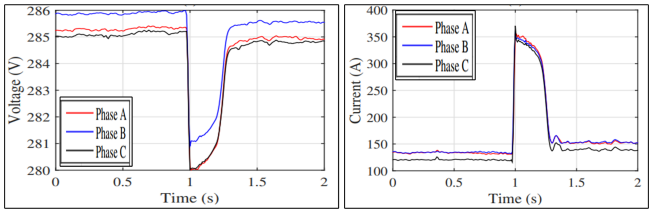

Figure 57. DG-switching event observed by the real μPMU [40].

5.4. Other Events

The remaining events are validated based on the fluctuations in load flow in the upstream and downstream μPMUs of the respective component because comprehensive observations of these events are not fully captured in the literature with regard to measurements of node voltage and line current. The validated data shows their applicability in developing and testing dedicated real-time DCC operational support applications for event detection, classification, and localization. This will help DCC operators with their daily planned and unplanned operations, as well as improving network reliability indices.

6. Experimental Use Case Test

To demonstrate the applicability of generated realistic μPMU data, a preliminary experimental study was carried out with the most relevant real-time use case.

Use Case: Event Classification

The real-time use case experimented in this section is the classification of an event that happened in the network. The experiment is to detect no-fault and fault events utilizing the μPMU data collected from the network. For this investigation, the line currents measured by the μPMUs are utilized. The below-mentioned basic algorithm is used to classify the events:

Step 1: Calculate the minimum short circuit currents (MSCC) of the network per phase.

Step 2: If the line currents measured by the master μPMU (μPMU1) per phase are greater than or equal to the MSCC of any phase, and if any of the μPMU measures a line current greater than 0.5 p.u. (threshold) for a duration of more than 20 ms or 0.020 s (this time duration is selected for use case test purposes only), then it is a "fault event"; otherwise, it is a "no-fault event".

The MSCC of phases A, B, and C are 0.2834 p.u., 0.2503 p.u., and 0.2343 p.u., respectively. Three-event data, such as tap changer (VR1), capacitor switching (844), and phase-to-ground fault (at 99.99% of line section "m" with 20 ohms), are used to test the data-driven approach. The results of these tests are shown in Table 9. The results show that the per-unit values of the line currents per phase for the tap changer and capacitor-switching events do not satisfy the conditions of the fault event, as the values do not touch the defined thresholds.

Table 9. Use case test results: fault and no-fault event classification.

Tested Data	Event Location	If Master μPMU $Value \geqslant MSSC$	If Any μPMU $Value \geqslant Threshold$	Classified Event
Tap Lowering	VR1	No	No	No-fault
A-G fault	At 99.99% of line section "m" with 20 ohms	Yes	Yes	Fault
Capacitor Off	844	No	No	No-fault

7. Conclusions

Realistic μPMU data generation for various real-time events in an unbalanced DN was successfully implemented using DP software. Realistic data were produced using real-time experience and combining μPMU elements in DP settings to fulfill the objectives of steady-state and dynamic data generation in an unbalanced benchmark DN. All potential real-time occurrences in the actual DN are covered by the created data, and the parameter variations are observed from their respective plots. Researchers can use this method to generate realistic data by reproducing the μPMU effect on the generated data because obtaining the original μPMU data can be difficult for a variety of reasons. Research and data-gathering times are reduced as a result. Additionally, realistic and useful data that match the replicated μPMU data are made available. This project's primary goal was to use the generated data for various μPMU use cases, including event detection, classification, and localization. Future studies will examine several studies to increase the usability of the data in research projects and incorporate various data quality issues into the generated data.

Author Contributions: Conceptualization, A.H.M.I.; methodology, A.H.M.I.; software, A.H.M.I.; validation, A.H.M.I.; formal analysis, M.S.; investigation, A.H.M.I.; resources, V.S.R.; data curation, A.H.M.I.; writing—original draft preparation, A.H.M.I.; writing—review and editing, M.S. and V.S.R.; visualization, V.S.R.; supervision, M.S. and V.S.R.; project administration, M.S.; funding acquisition, V.S.R. All authors have read and agreed to the published version of the manuscript.

Funding: This research was funded by the Transnational Access program of the EU H2020 ERIGrid 2.0 project with grant agreement number 870620.

Data Availability Statement: The data and functional details presented in this study are available upon request from the corresponding author.

Acknowledgments: The authors are thankful to W. H. Kersting for his email assistance in the perfect modeling of the IEEE 34 test feeder and associated load flow analysis validations in DIgSILENT PowerFactory. The researchers would like to acknowledge the Intelligent Electrical Power Grids Group at Technische Universiteit Delft in the Netherlands, as well as their technical and administrative staff, for their assistance and direction in remotely accessing the lab facilities.

Conflicts of Interest: The authors declare that there are no potential conflict of interest in the research, authorship, or publication of this article.

Abbreviations

The following abbreviations are used in this manuscript:

μPMU	Micro-Phasor Measurement Unit
DER	Distributed Energy Resources
DN	Distribution Network
ROCOF	Rate of Change of Frequency
DP	DIgSILENT PowerFactory
SCADA	Supervisory Control and Data Acquisition
RTU	Remote Terminal Unit
GPS	Global Positioning System
DCC	Distribution Control Centre
DG	Distributed Generation
LV	Low Voltage
DT	Distribution Transformer
OHL	Overhead Lines
IEEE	Institute of Electrical and Electronics Engineers
PES	Power and Energy Society
DSAC	Distribution System Analysis Committee
NR	Newton–Raphson
CSORI	Complete System Observability Redundancy Index
CI	Cost Index
CB	Circuit Breaker
US	Upstream
DS	Downstream
XF10	Line Transformer
S Capacitor	Shunt Capacitor
SL	Spot Load
DL	Distributed Load
MCB	Miniature Circuit Breaker
MSCC	Minimum Short Circuit Current

Appendix A

Table A1. Line section representation for IEEE 34 node model in DIgSILENT Powerfactory.

Line Section	Node (i)	Node (j)
A	800	802
B	802	802′
C	802′	806
D	806	808
E	808	812
F	812	814
G	RG10	850
H	850	816
I	816	816′
J	816′	824
K	824	824′
L	824′	828
M	828	828′
N	828′	830
O	830	854
P	854	852
Q	RG11	832
R	832	832′
S	832′	858
T	858	858′
U	858′	834
V	834	834′
W	834′	860
X	860	860′
Y	860′	836
Z	836	836′
a	836′	840
b	808	808′
c	808′	810
d	816	818
e	818	818′
f	818′	820
g	820	820′
h	820′	822
i	824	824′
j	824′	826
k	854	854′
l	854′	856
m	888	890
n	858	858′
o	858′	864
p	834	842
q	842	842′
r	842′	844
s	844	844′
t	844′	846
u	846	846′
v	846′	848
w	836	862
x	862	862′
y	862′	838

Table A2. Load flow results from DP model (node voltages and angles per phase).

Node	Uln, Magnitude A (p.u.)	Uln, Magnitude B (p.u.)	Uln, Magnitude C (p.u.)	Uln, Angle A (deg)	Uln, Angle B (deg)	Uln, Angle C (deg)
802	1.047	1.048	1.048	−0.05	−120.06	119.95
806	1.046	1.047	1.047	−0.09	−120.11	119.91
808	1.014	1.03	1.029	−0.75	−120.95	119.3
810		1.03			−120.95	
812	0.976	1.01	1.007	−1.58	−121.92	118.58
814	0.947	0.995	0.989	−2.27	−122.7	118.01
816	1.017	1.025	1.02	−2.28	−122.71	118
818	1.016			−2.28		
820	0.99			−2.3		
822	0.99			−2.35		
824	1.008	1.016	1.012	−2.39	−122.93	117.75
826		1.016			−122.94	
828	1.007	1.015	1.011	−2.4	−122.95	117.73
830	0.989	0.998	0.994	−2.66	−123.39	117.23
832	1.036	1.035	1.036	−3.14	−124.18	116.32
834	1.031	1.03	1.031	−3.27	−124.38	116.07
836	1.03	1.029	1.031	−3.26	−124.38	116.07
838		1.029			−124.39	
840	1.03	1.029	1.031	−3.26	−124.38	116.07
842	1.031	1.03	1.031	−3.27	−124.38	116.06
844	1.031	1.029	1.031	−3.29	−124.41	116.03
846	1.031	1.029	1.031	−3.33	−124.45	115.97
848	1.031	1.029	1.031	−3.34	−124.45	115.96
850	1.018	1.026	1.02	−2.27	−122.7	118.01
852	0.958	0.968	0.964	−3.14	−124.18	116.32
854	0.989	0.998	0.993	−2.66	−123.4	117.22
856		0.998			−123.41	
858	1.033	1.032	1.034	−3.2	−124.27	116.21
860	1.03	1.029	1.031	−3.26	−124.38	116.06
862	1.03	1.029	1.031	−3.26	−124.38	116.07
864	1.033			−3.2		
888	0.999	0.999	1	−4.67	−125.73	114.8
890	0.917	0.923	0.918	−5.15	−126.79	113.91
DG802_BB	0	0	0	0	0	0
DG840_BB	0	0	0	0	0	0
DG848_BB	0	0	0	0	0	0
DG850_BB	0	0	0	0	0	0
DG852_BB	0	0	0	0	0	0
DG862_BB	0	0	0	0	0	0
RG10	1.018	1.026	1.02	−2.27	−122.7	118.01
RG11	1.036	1.035	1.036	−3.14	−124.18	116.32
RG11	1.036	1.035	1.036	−3.1	−124.2	116.3

Table A3. Load flow results from DP model (line currents and angles per phase).

Line Section	Phase Current, Magnitude A (A)	Phase Current, Magnitude B (A)	Phase Current, Magnitude C (A)	Phase Current, Angle A (deg)	Phase Current, Angle B (deg)	Phase Current, Angle C (deg)
A	51.6	44.6	40.9	−12.74	−127.67	117.32
B	51.6	44.6	40.9	−12.79	−127.73	117.26
C	51.6	42.5	39.2	−12.81	−126.78	118.48
D	51.6	42.5	39.2	−12.83	−126.8	118.46
E	51.8	41.3	39.3	−13.46	−127.07	117.71
F	52	41.3	39.3	−14.18	−127.97	116.85
G	48.5	40	38.2	−14.73	−128.67	116.18
H	48.5	40	38.2	−14.73	−128.67	116.18
I	35.8	40	38.2	−10.43	−128.67	116.17
J	35.9	39.8	38	−10.57	−128.87	116.31
K	35.9	36.9	38	−10.7	−127.36	116.19
L	35.9	36.9	37.8	−10.72	−127.37	116.38
M	35.9	36.9	37.8	−10.73	−127.38	116.37
N	35.4	36.9	37.8	−10.79	−127.64	116.14
O	34.2	36.2	36.5	−9.98	−127.44	116.21
P	34.2	35.9	36.5	−9.99	−127.69	116.2

Table A3. *Cont.*

Line Section	Phase Current, Magnitude A (A)	Phase Current, Magnitude B (A)	Phase Current, Magnitude C (A)	Phase Current, Angle A (deg)	Phase Current, Angle B (deg)	Phase Current, Angle C (deg)
Q	31.8	33.6	34	−11.01	−128.63	115.35
R	21.3	23.4	24.3	0.44	−116.87	128.32
S	20.9	23.1	24	0.95	−116.27	128.54
T	20.7	23.1	24	0.98	−116.37	128.45
U	20.3	22.4	23.2	2.3	−115.92	130.14
V	11.2	9.1	10.6	−43.07	−154.82	99.32
W	5.9	7.7	5.3	−33.49	−156.41	86.22
X	4.2	6	3.6	−30.2	−154.63	90.23
Y	1.5	4.4	1.7	−18.98	−150.47	68.5
Z	1.5	2.3	1.7	−20.02	−151.97	67.98
a	0.8	0.8	0.8	−40.72	−161.81	78.55
b		1.2			−144.6	
c		0			−30.95	
d	13			−26.66		
e	13			−26.74		
f	10.5			−27.6		
g	10.6			−28.96		
h	0.1			87.67		
i		3.1			−148.91	
j		0			−32.94	
k		0.3			−98.38	
l		0.1			−33.41	
m	69.9	70	69.5	−32.3	−152.74	87.37
n	0.1			−22.8		
o	0			86.8		
p	14.7	16.3	15.1	34.63	−95.6	151.02
q	14.7	16.3	15.1	34.62	−95.61	151.01
r	14.5	16.3	15.1	37.11	−95.64	150.97
s	9.8	9.4	9.4	78.83	−63.85	−170.68
t	9.8	9.4	9.8	78.8	−52.49	−161.91
u	9.8	9.4	9.8	78.76	−52.53	−161.94
v	9.8	9.8	9.8	78.75	−42.46	−161.95
w	0	2.1	0	90.43	−149.37	−150.76
x		2.1			−149.49	
y		0			−34.39	

Table A4. List of realistic real-time events generated using DP in the test feeder.

Sl. No	Event Execution Time(s) on 21 August 2022 11:00 AM	Event Description *	Event Location	Event Category
1	40.05	Unbalanced Voltage complaint from SL 890	SL 890	Unbalanced voltage
2	52.05	Rectification of Unbalanced Voltage from SL 890	SL 890	Unbalanced voltage rectification
3	54	XF10 DE-ENERGIZED for Maintenance	XF10	Transformer outage
4	74	VR2 Tap Lowered (13-11-12 to 12-10-11)	VR2	Tap changer event
5	94	VR2 Tap Lowered (12-10-11 to 11-09-10)	VR2	Tap changer event
6	114	VR2 Tap Lowered (11-09-10 to 10-08-09)	VR2	Tap changer event
7	134	VR2 Tap Lowered (10-08-09 to 09-07-08)	VR2	Tap changer event
8	154	VR2 Tap Lowered (09-07-08 to 08-06-07)	VR2	Tap changer event
9	174	Cap844 Switch Off	S Capacitor 1	Capacitor bank event
10	194	DG848 Switch On	DG848	DG-switching event
11	214	C-G Fault 20ohm Temporary Fault at A	A	Temporary fault event
12	214.04	Main Feeder Circuit Breaker Tripped on C-G Fault	Main Feeder Circuit Breaker	CB trip event
13	214.135	C-G Temporary Fault Cleared	A	Fault clearing

Table A4. *Cont.*

Sl. No	Event Execution Time(s) on 21 August 2022 11:00 AM	Event Description *	Event Location	Event Category
14	234.185	Main Feeder Circuit Breaker Reclosed	A	CB-switching event
15	254.185	Heavy Load 844 (3PH) Switch Off	SL 844	Load trip event
16	274.185	B-N Jumper Parted OpenCircuit Flt808-810	808-810 B-N Jumper	Open circuit fault event
17	294.185	XF10 ENERGIZED After Maintenance	XF10	Transformer energization
18	314.185	DG848 Switch Off	DG848	DG-switching event
19	334.185	3Phase Short-Circuit Fault 10 ohms at G	G	Short circuit fault event
20	334.225	Main Feeder Circuit Breaker Tripped on ABC SC Fault	Main Feeder Circuit Breaker	CB trip event
21	354.225	Fault Rectified and Cable Kept in Service	G	Fault Clearing
22	374.225	Main Feeder Circuit Breaker Closed_1	Main Feeder Circuit Breaker	CB-switching event
23	394.225	DG840 Switch On	DG840	DG-switching event
24	414.225	ABC Short-Circuit Fault 10 ohm at G DG840	G	Short circuit fault event
25	414.265	Main Feeder Circuit Breaker Tripped on ABC SC wDG840	Main Feeder Circuit Breaker	CB trip event
26	434.265	Fault Rectified and Cable Kept in Srvc	G	Fault clearing
27	454.265	Main Feeder Circuit Breaker Closed_2	Main Feeder Circuit Breaker	CB-switching event
28	474.265	VR1 Tap Lowered (12-05-05 to 13-06-06)	VR1	Tap changer event
29	494.265	DG840 Switch Off	DG840	DG-switching event
30	514.265	A-B Fault 10ohms at O	O	Short circuit fault event
31	514.305	Main Feeder Circuit Breaker Tripped on A-B Fault	Main Feeder Circuit Breaker	CB trip event
32	534.048	Fault Rectified and Cable Kept in SRVC	O	Fault clearing
33	554.048	Main Feeder Circuit Breaker Closed_3	Main Feeder Circuit Breaker	CB-switching event
34	574.048	Customer requested outage at SL848	SL 848	Load-switching event
35	594.048	Cap 848 Switch Off	S Capacitor 2	Capacitor bank Event
36	614.048	OHL section D De-energized 4 Jumper Connection	D	Line De-energization
37	634.048	OHL section E De-energized 4 Jumper Connection	E	Line energization
38	654.048	B-N Jumper 808-810 Connected	808-810 B-N Jumper	OHL jumper connection
39	674.048	OHL section E Connected for engzn	E	Line energization
40	694.048	OHL section D Connected and Svc restd2al	D	Line energization
41	714.048	DG852 Switched On	DG852	DG-switching event
42	734.048	A_G Fault at A	A	Short circuit fault event
43	734.088	DG852 Tripped on A-G Fault	CB	DG trip event
44	734.128	Main Feeder Circuit Breaker Tripped on A-G Fault	Main Feeder Circuit Breaker	CB trip event
45	754.128	Fault Rectified and Cable Kept in SVC	A	Fault clearing
46	774.128	Main Feeder Circuit Breaker Closed_4	A	CB-switching event
47	794.128	B-C Jumper OP between 834-842	p	OHL jumper opening
48	814.128	B_C Fault at p	p	Short circuit fault event
49	814.168	Main Feeder Circuit Breaker Tripped on BC SC Fault	Main Feeder Circuit Breaker	CB trip event
50	834.168	SC Fault Cleared	p	Fault Clearing
51	854.168	Jumper Closed 834 to 842	Jumper	OHL jumper connection
52	874.168	Main Feeder Circuit Breaker Closed_5	Main Feeder Circuit Breaker	CB-switching event

Table A4. *Cont.*

Sl. No	Event Execution Time(s) on 21 August 2022 11:00 AM	Event Description *	Event Location	Event Category
53	894.168	DG 850 Switched On	DG850	DG-switching event
54	914.168	BCN Load Trip Event	DL 802-806	Load trip event
55	934.168	A-B-G Fault at F	F	Short circuit fault event
56	934.208	DG850 Tripped	DG850	DG trip event
57	934.248	Main Feeder Circuit Breaker tripped on A-B-G Fault	Main Feeder Circuit Breaker	CB trip event
58	954.248	A-B-G Fault Cleared	F	Fault clearing
59	974.248	Main Feeder Circuit Breaker Closed_6	Main Feeder Circuit Breaker	CB-switching event
60	994.248	C-phase of DL 834-860 Tripped	DL 834-860	Load trip event
61	1014.248	MCB of C-phase Closed for DL 834-860	DL 834-860	Load-switching event
62	1034.248	DG802 Switched On	DG802	DG-switching event
63	1054.248	DG840 Switched On Generation Increased	DG840	DG-switching event
64	1074.248	ABCN-G Fault at L	L	Short circuit fault event
65	1074.288	DG840 Tripped	DG840	DG trip event
66	1074.328	DG802 Tripped	DG802	DG trip event
67	1074.368	Main Feeder Circuit Breaker Tripped on ABCG Fault	Main Feeder Circuit Breaker	CB trip event
68	1094.368	ABCG Fault Cleared	L	Fault Clearing
69	1114.368	Main feeder Circuit Breaker Closed07	Main Feeder Circuit Breaker	CB-switching event
70	1134.368	2 PH YN load Switched On (DL 802-806)	DL 802-806	Load-switching event
71	1154.368	2 PH YN load Switched Off (DL 844-846)byC	DL 844-846	Load-switching event
72	1174.368	2 PH YN load Switched On (DL 844-846)by C	DL 844-846	Load-switching event
73	1194.368	B-G Fault 10 ohms at m	m	Short circuit fault event
74	1194.408	XF10 Tripped	XF10	Transformer trip event
75	1214.408	B-C-G Fault 10 ohms at q	q	Short circuit fault event
76	1214.448	Main Feeder Circuit Breaker Tripped on B-C-G Fault	Main Feeder Circuit Breaker	CB trip event
77	1234.448	B-C-G Fault Cleared	q	Fault Clearing
78	1254.448	Main Feeder Circuit Breaker Closed_8	Main Feeder Circuit Breaker	CB-switching event
79	1274.448	A-N load Switch Off (DL 820-822)	DL 820-822	Load-switching event
80	1294.448	C-A Fault 10 ohms at B	B	Short circuit fault event
81	1294.488	Main Feeder Circuit Breaker Tripped on C-A Fault	Main Feeder Circuit Breaker	CB trip event
82	1314.488	C-A Fault Cleared	B	Fault clearing
83	1334.488	Main Feeder Circuit Breaker Closed_9	Main Feeder Circuit Breaker	CB-switching event
84	1354.488	B-G Fault Cleared at m	m	Fault clearing
85	1374.488	XF10 Switched On	XF10	Transformer energization
86	1394.488	DG852 Switch On	DG852	DG-switching event
87	1414.488	VR2 Tap Raised (08-06-07 to 09-07-08)	VR2	Tap changer event
88	1434.488	VR2 Tap Raised (09-07-08 to 10-08-09)	VR2	Tap changer event
89	1454.488	VR2 Tap Raised (10-08-09 to 11-09-10)	VR2	Tap changer event
90	1474.488	VR2 Tap Raised (11-09-10 TO 12-10-11)	VR2	Tap changer event
91	1494.488	VR2 Tap Raised (12-10-11 to 13-11-12)	VR2	Tap changer event
92	1514.488	DG852 Switch Off	DG852	DG-switching event
93	1534.488	C-A-G Fault 10 ohms at A	A	Short circuit fault event
94	1534.528	Main Feeder Circuit Breaker Tripped on C-A-G Fault	Main Feeder Circuit Breaker	CB trip event
95	1554.528	C-A-G Fault Cleared at A	A	Fault clearing
96	1574.528	Main Feeder Circuit Breaker Closed	Main Feeder Circuit Breaker	CB-switching event

Table A4. *Cont.*

Sl. No	Event Execution Time(s) on 21 August 2022 11:00 AM	Event Description *	Event Location	Event Category
97	1594.528	A-N load Switch On (DL 820-822)	DL 820-822	Load-switching event
98	1614.528	C-G Fault 10 ohms at A	A	Short circuit fault event
99	1614.568	Main Feeder Circuit Breaker Tripped onC-G Fault	Main Feeder Circuit Breaker	CB trip event
100	1634.568	C-G Fault cleared at A	A	Fault clearing
101	1654.568	Main Feeder Circuit Breaker Closed	Main Feeder Circuit Breaker	CB-switching event
102	1674.568	Low Voltage Complaint from SL 890	SL 890	LV complaint
103	1694.568	VR1 Tap Raised (13-06-06 to 14-07-07)	VR1	Tap changer event
104	1714.568	VR1 Tap Raised (14-07-07 to 15-08-08)	VR1	Tap changer event
105	1734.568	SL 890 Energized after V regulation	SL 890	Load-switching event
106	1740.568	Cap844 Switch On	S Capacitor 1	Capacitor bank event
107	1746.025	SL 844 Switch On	SL 844	Load-switching event
108	1777.123	SL 848 Switch On	SL 848	Load-switching event
109	1799.001	Cap848 Switch On	S Capacitor 2	Capacitor bank event

* A, B, C, N,and G are Phases A, B, C, Neutral, and Ground respectively.

Appendix B

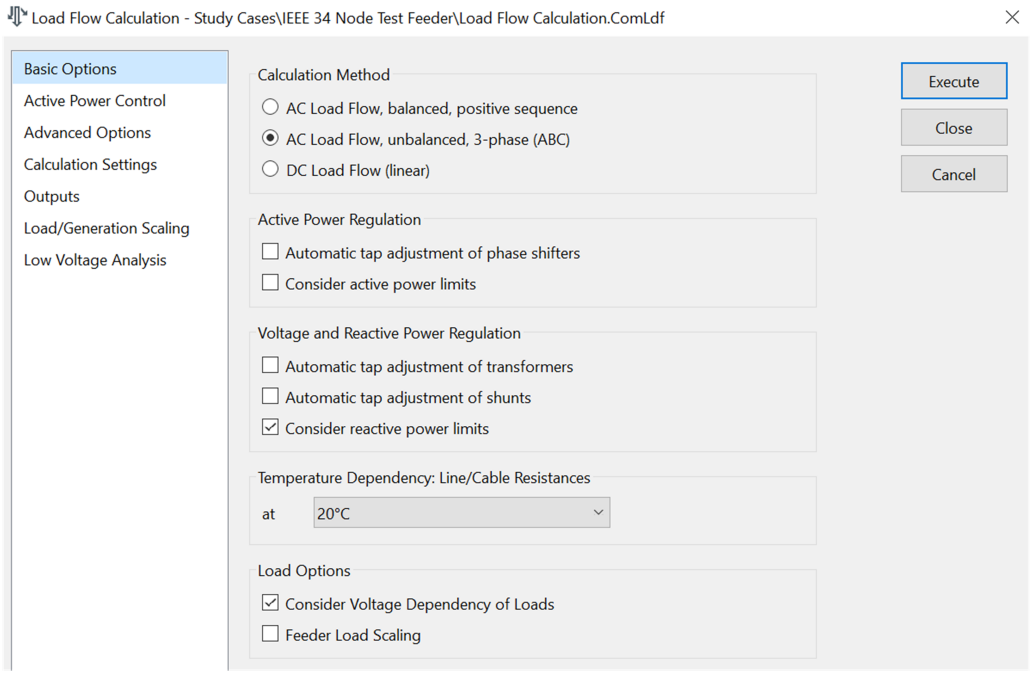

Figure A1. Load flow basic settings.

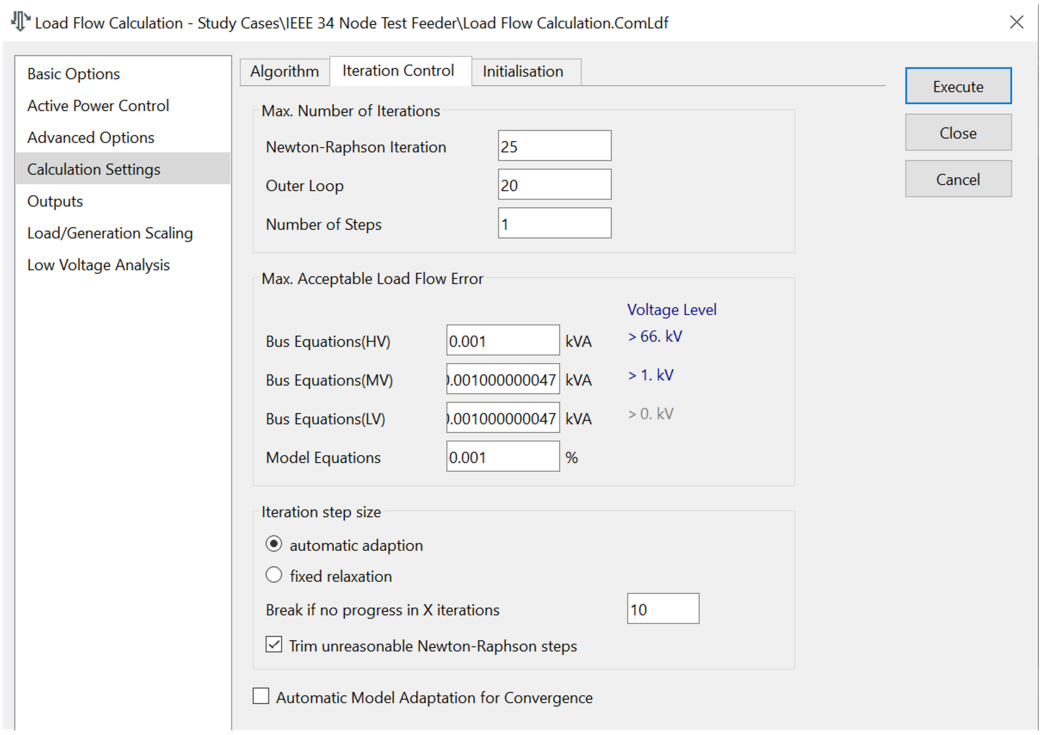

Figure A2. Load flow iteration control settings.

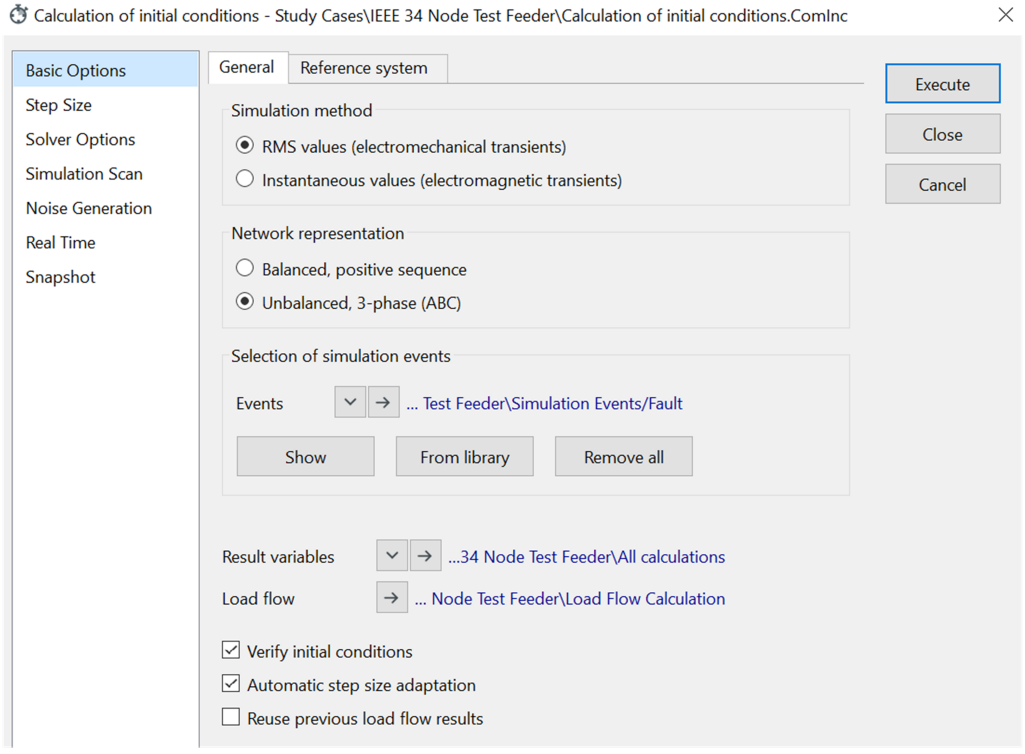

Figure A3. RMS Simulation basic settings.

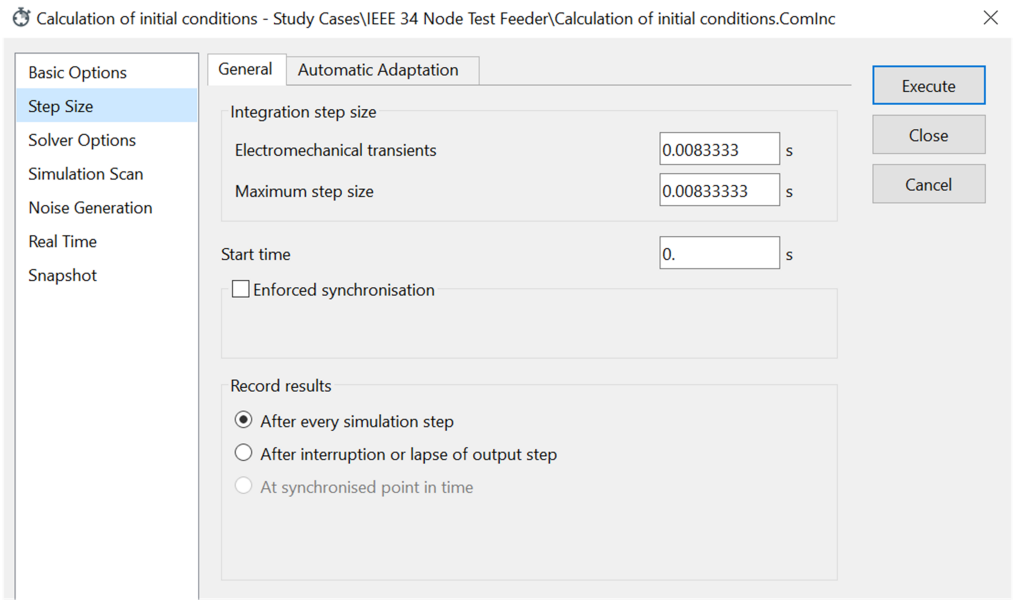

Figure A4. Data generation step size settings1.

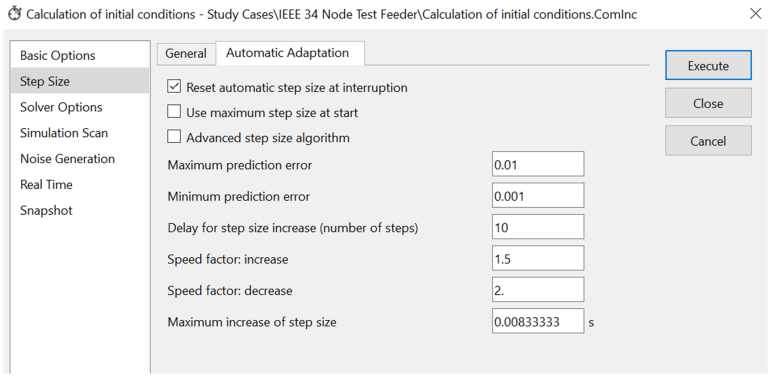

Figure A5. Data generation step size settings2.

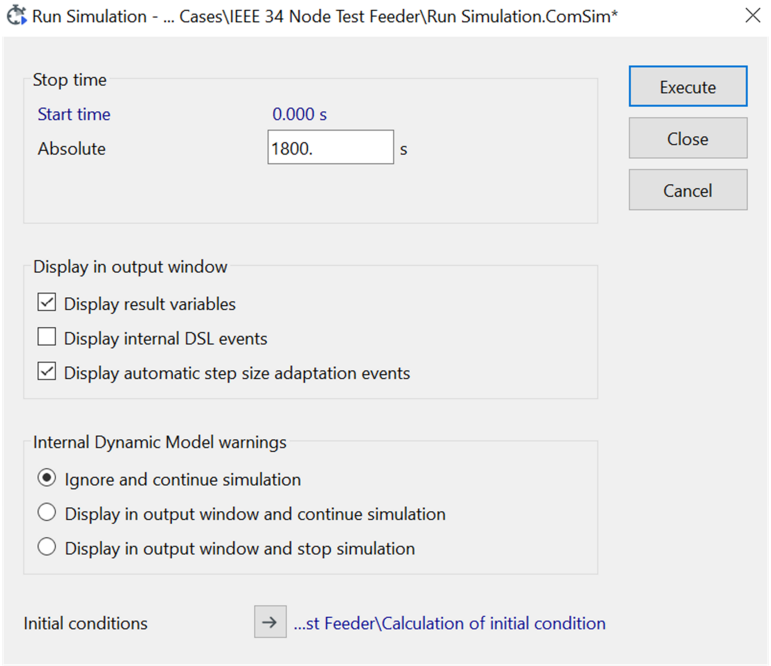

Figure A6. Run Simulation Settings.

References

1. Von Meier, A.; Stewart, E.; McEachern, A.; Andersen, M.; Mehrmanesh, L. Precision μ-Synchrophasors for Distribution Systems: A Summary of Applications. *IEEE Trans. Smart Grid* **2017**, *2*, 2926–2936.
2. Dusabimana, E.; Yoon, S.-G. A Survey on the μ-Phasor Measurement Unit in Distribution Networks. *Energies* **2020**, *9*, 305.
3. Shahsavari, A.; Farajollahi, M.; Stewart, E.M.; Cortez, E.; Mohsenian-Rad, H. Situational Awareness in Distribution Grid Using μPMU Data: A Machine Learning Approach. *IEEE Trans. Smart Grid* **2019**, *10*, 6167–6177.
4. Energy Technologies Area. Available online: https://eta-publications.lbl.gov/sites/default/files/lbnl-1006408_open_u$\upmu$PMU_ieee_oct2016.pdf (accessed on 13 November 2022).
5. Haridas, R.P. GPS Based Phasor Technology in Electrical Power System. *IJEEE* **2014**, *3*, 493–496.
6. Power Standards Lab. Introduction to μPMU. Available online: www.powerstandards.com\protect\T1\textdollar/wpcontent/uploads/dlm_uploads/2017/10/\protect\T1\textdollarIntroduction-to-$\upmu$$\upmu$PMU.pdf (accessed on 13 November 2022).
7. Lee, L.; Centeno, V. Comparison of mμPMU and μPMU. In Proceedings of the Clemson University Power Systems Conference (PSC), Charleston, SC, USA, 4–7 December 2018; pp. 1–6.
8. Kummerow, A.; Rösch, D.; Monsalve, C.; Nicolai, S.; Bretschneider, P.; Brosinsky, C.; Westermann, D. Challenges and Opportunities for Phasor Data Based Event Detection in Transmission Control Centers under Cyber Security Constraints. In Proceedings of the 2019 IEEE Milan PowerTech, Milan, Italy, 23–27 June 2019; pp. 1–6.
9. Sajan, K.S.; Bariya, M.; Basak, S.; Srivastava, A.; Dubey, A.; von Meier, A.; Biswas, G. Realistic Synchrophasor Data Generation for Anomaly Detection and Event Classification. In Proceedings of the 2020 8th Workshop on Modeling and Simulation of Cyber-Physical Energy Systems, Sydney, NSW, Australia, 21 April 2020; pp. 1–6.
10. Shahsavari, A.; Farajollahi, M.; Stewart, E.; Roberts, C.; Megala, F.; Alvarez, L.; Cortez, E.; Mohsenian-Rad, H. Autopsy on active distribution networks: A data-driven fault analysis using μPMU data. In Proceedings of the 2017 North American Power Symposium (NAPS), Morgantown, WV, USA, 17–19 September 2017; pp. 1–7.
11. Aligholian, A.; Shahsavari, A.; Stewart, E.M.; Cortez, E.; Mohsenian-Rad, H. Unsupervised Event Detection, Clustering, and Use Case Exposition in μPMU Measurements. *IEEE Trans. Smart Grid* **2021**, *12*, 3624–3636.
12. Soltani, Z.; Khorsand, M. Real-Time Topology Detection and State Estimation in Distribution Systems Using μPMU and Smart Meter Data. *IEEE Syst. J.* **2022**, *16*, 3554–3565.
13. Khaledian, P.; Mohsenian-Rad, H. Automated Event Region Identification and Its Data-Driven Applications in Behind-the-Meter Solar Farms Based on μPMU Measurements. *IEEE Trans. Smart Grid* **2022**, *13*, 2094–2106.
14. Bu, F.; Dehghanpour, K.; Wang, Z. Enriching Load Data Using μPMUs and Smart Meters. *IEEE Trans. Smart Grid* **2021**, *12*, 5084-5094.
15. Shahsavari, A.; Farajollahi, M.; Stewart, E.; von Meier, A.; Alvarez, L.; Cortez, E.; Mohsenian-Rad, H. A data-driven analysis of capacitor bank operation at a distribution feeder using μPMU data. In Proceedings of the 2017 IEEE Power & Energy Society Innovative Smart Grid Technologies Conference (ISGT), Washington, DC, USA, 23–26 April 2017; pp. 1–5.
16. Farajollahi, M.; Shahsavari, A.; Stewart, E.M.; Mohsenian-Rad, H. Locating the Source of Events in Power Distribution Systems Using μPMU Data. *IEEE Trans. Power Syst.* **2018**, *33*, 6343–6354.
17. Zhang, Y.; Wang, J.; Khodayar, M.E. Graph-Based Faulted Line Identification Using μPMU Data in Distribution Systems. *IEEE Trans. Smart Grid* **2020**, *11*, 3982–3992.
18. Sanitha, G.; Shereef, R.M. μPMU data based location identification and classification of events. In Proceedings of the 2020 IEEE International Conference on Power Electronics, Smart Grid and Renewable Energy (PESGRE2020), Cochin, India, 2–4 January 2020; pp. 1–6.
19. Duan, N.; Stewart, E.M. Frequency Event Categorization in Power Distribution Systems Using μPMU Measurements. *IEEE Trans. Smart Grid* **2020**, *11*, 3043–3053.
20. Stewart, E.M.; Kiliccote, S.; Shand, C.M.; McMorran, A.W.; Arghandeh, R.; von Meier, A. Addressing the challenges for integrating micro-synchrophasor data with operational system applications. In Proceedings of the 2014 IEEE PES General Meeting & Exposition, National Harbor, MD, USA, 27–31 July 2014; pp. 1–5.
21. Jacob, R.A.; Paul, S.; Li, W.; Chowdhury, S.; Gel, Y.R.; Zhang, J. Reconfiguring Unbalanced Distribution Networks using Reinforcement Learning over Graphs. In Proceedings of the 2022 IEEE Texas Power and Energy Conference (TPEC), College Station, TX, USA, 28 February–1 March 2022; pp. 1–6.
22. Dashti, R.; Ghasemi, M.; Daisy, M. Fault location in power distribution network with presence of distributed generation resources using impedance based method and applying π line model. *Energy* **2018**, *159*, 344–360.
23. Haleem, A.M.I.; Sharma, M.; Sajan, K.S.; Babu, K.N.D. A Comparative Review of Fault Location/Identification Methods in Distribution Networks. In Proceedings of the 2018 1st International Conference on Advanced Research in Engineering Sciences (ARES), Dubai, United Arab Emirates, 15 June 2018; pp. 1–6.
24. Kersting, W. Radial distribution test feeders. *IEEE Trans. Power Syst.* **2001**, *2*, 908–912.
25. Radial Distribution Test Feeders. Available online: http://ewh.ieee.org/soc/pes/dsacom/testfeeders.html (accessed on 13 November 2022).
26. Digsilent Powerfactory 2022 Technical References. Available online: https://www.digsilent.de/en/powerfactory-download.html?folder=files%2Fdownloads%2Fprivate%2F10_PowerFactory%2F10_PowerFactory_2022%2F70_Technical+References (accessed on 13 November 2022).

27. IEEE. *IEEE Tutorial Course on Distribution Automation*; 88 EH0280-8 PWR; IEEE Power Engineering Society: Piscataway, NJ, USA, 1988.
28. IEEE. *IEEE Tutorial Course on Power Distribution Planning*; 92 EHO 381-6 PWR; IEEE Power Engineering Society: Piscataway, NJ, USA, 1992.
29. Birt, K.A.; Graffy, J.J.; McDonald, J.D.; El-Abiad, A.H. Three phase load flow program. *IEEE Trans. Power Appar. Syst.* **1976**, *952*, 59–65.
30. Chen, T.H.; Chen, M.S.; Hwang, K.-J.; Kotas, P.; Chebli, E.A. Distribution system power flow analysis-A rigid approach. *IEEE Trans. Power Deliv.* **1991**, *6*, 1146–1152.
31. Chen, T.H.; Chen, M.S.; Inoue, T.; Chebli, E.A. Three-phase cogenerator and transformer models for distribution system analysis. *IEEE Trans. Power Deliv.* **1991**, *6*, 1671–1681.
32. Lin, W.M.; Teng, J.H. Three-phase distribution network fast decoupled power flow solution. *Int. J. Elect. Power Energy Syst.* **2000**, *5*, 375–380.
33. Teng, J.-H.; Chang, C.-Y. A novel and fast three-phase load flow for unbalanced radial distribution systems. *IEEE Trans. Power Syst.* **2002**, *17*, 1238–1244.
34. Kotha, S.K.; Rajpathak, B.; Ramesh, B.; Khedkar, M.K. Optimal Placement of μPMUs for Real-time Monitoring of Inter-Connected Smart Distribution Networks. In Proceedings of the 2nd Asian Conference on Innovation in Technology (ASIANCON), Ravet, India, 26–28 August 2022; pp. 1–5.
35. Tahabilder, A.; Ghosh, P.K.; Chatterjee, S.; Rahman, N. Distribution system monitoring by using μPMU in graph theoretic way. In Proceedings of the 2017 4th International Conference on Advances in Electrical Engineering (ICAEE), Dhaka, Bangladesh, 28–30 September 2017; pp. 159–163.
36. Chen, X.; Chen, T.; Tseng, K.J.; Sun, Y.; Amaratunga, G. Hybrid approach based on global search algorithm for optimal placement of μPMU in distribution networks. In Proceedings of the 2016 IEEE Innovative Smart Grid Technologies—Asia (ISGT-Asia), Melbourne, VIC, Australia, 28 November–1 December 2016; pp. 559–563.
37. Jamil, E.; Rihan, M.; Anees, M.A. Towards optimal placement of phasor measurement units for smart distribution systems. In Proceedings of the 2014 6th IEEE Power India International Conference (PIICON), Delhi, India, 5–7 December 2014; pp. 1–6.
38. Silva, J.A.; Funmilayo, H.B.; Bulter-Purry, K.L. Impact of Distributed Generation on the IEEE 34 Node Radial Test Feeder with Overcurrent Protection. In Proceedings of the 2007 39th North American Power Symposium, Las Cruces, NM, USA, 30 September–2 October 2007; pp. 49–57.
39. Short, T.A. *Electric Power Distribution Handbook*, 2nd ed.; CRC Press: Boca Raton, FL, USA, 2014.
40. Shahsavari, A. Data-Driven Analysis of Power Distribution Synchrophasors with Applications to Situational Awareness, Load Modeling, and Reliability. Ph.D. Thesis, University of California, Riverside, CA, USA, September 2019.